
Detecting Transportation Mode Using Dense Smartphone GPS Trajectories and Transformer Models

Yuandong Zhang*
University of California
San Diego, CA, USA

Othmane Echchabi*
McGill University
Mila - Quebec AI Institute
Montréal, QC, Canada

Tianshu Feng
University of Pennsylvania
Philadelphia, PA, USA

Wenyi Zhang
Duke Kunshan University
Kunshan, Jiangsu, China

Hsuai-Kai Liao
Duke Kunshan University
Kunshan, Jiangsu, China

Charles Chang[†]
Duke Kunshan University
Kunshan, Jiangsu, China

Abstract

Transportation mode detection is an important topic within GeoAI and transportation research. In this study, we introduce SPEEDTRANSFORMER, a novel Transformer-based model that relies solely on speed inputs to infer transportation modes from dense smartphone GPS trajectories. In benchmark experiments, SPEEDTRANSFORMER outperformed traditional deep learning models, such as the Long Short-Term Memory (LSTM) network. Moreover, the model demonstrated strong flexibility in transfer learning, achieving high accuracy across geographical regions after fine-tuning with small datasets. Finally, we deployed the model in a real-world experiment, where it consistently outperformed baseline models under complex built environments and high data uncertainty. These findings suggest that Transformer architectures, when combined with dense GPS trajectories, hold substantial potential for advancing transportation mode detection and broader mobility-related research.

Keywords: GeoAI; Transformers; Dense GPS Trajectories; Deep Learning; Field Experiments; Emissions.

1 Introduction

The study of human mobility patterns—how individuals move across space—has become an important topic across geography, transportation science, public health, and climate change science [1; 2; 3; 4; 5; 6; 7; 8; 9; 10]. One key aspect of human mobility is transportation mode choice, the accurate estimation of which is essential for understanding individual carbon emissions and associated health benefits [11; 12].

*These authors contributed equally to this work.

[†]Corresponding author. Email: charles.c.chang@dukekunshan.edu.cn

Traditionally, transportation surveys were used to estimate individual’s choices of transportation mode [13]. However, two major technological advancements in recent years have reshaped transportation mode detection. First, smartphones—equipped with GPS, accelerometers, gyroscopes, and cellular network connectivity—have enabled the creation of detailed mobility datasets derived from mobile applications [14], social media platforms [15], travel cards [16], and cellphone signals [17]. These datasets surpassed traditional transportation surveys in dimensionality, accuracy, variety, and volume [18; 19].

Second, advancements in machine learning (ML) have greatly improved the ability to extract meaningful information from mobility datasets. Machine learning techniques—from ensemble methods to deep learning models—now exploit increasingly fine-grained spatiotemporal data, including human mobility traces, substantially improving the accuracy of transportation-mode prediction [20]. More recently, Transformer [21] architectures are adopted for human mobility research given their self-attention mechanisms, which can help capture nonlinear spatiotemporal dependencies and high-order motion features. Furthermore, their capacity for inductive transfer enables cross-regional generalization, potentially allowing models to adapt to diverse transportation infrastructures using minimal labeled data.

Nevertheless, significant challenges remained. Smartphone-derived mobility datasets, while highly granular, often exhibited inconsistent quality due to the absence of standardized data collection protocols and inaccuracies in geographic information, complicating modeling process. Model performance frequently depended on derived features such as acceleration, while complex preprocessing tasks—such as geocoding and geotagging—further increased data uncertainty. Moreover, extensive feature engineering used to aggregate raw GPS trajectories often resulted in the loss of critical sequential information essential for accurate mobility modeling [22].

Privacy posed another major challenge. Mobility applications commonly collected sensitive information, including geographic locations, trip details (e.g., start and end times), and personal or device identifiers. For example, Xu et al. [23] demonstrated that even anonymized mobility data could be re-identified with 73–91% accuracy, underscoring the difficulty of ensuring privacy protection. Such risks frequently discouraged individuals from sharing their mobility data [24], constraining data availability.

Moreover, mobility models have often lacked generalizability across geographic regions, particularly when trained on isolated or geographically homogeneous datasets. Human mobility behaviors vary widely across countries and regions due to differences in road infrastructure, speed regulations, and cultural norms. Nevertheless, most studies have assessed model performance using train–test splits from the same dataset [25], which fail to capture real-world adaptability. Models fine-tuned on benchmarks such as Geolife [26] frequently required substantial recalibration when applied to other contexts. The proliferation of deep learning frameworks, hyperparameter tuning strategies, and architectural variations has further complicated cross-regional reproducibility in mobility modeling research [27].

Finally, existing mobility models have often struggled to perform reliably under real-world conditions, which are considerably more unpredictable and complex than curated research datasets suggest. Everyday travel involves nuances such as short trips and unexpected errands that traditional models frequently misclassified [20]. Moreover, GPS signal quality varied across smartphone models and was highly sensitive to environmental factors, including urban canyons and signal obstructions [28; 29]. These real-world data inconsistencies—typically underrepresented in benchmark datasets—underscore the need to validate mobility models under realistic conditions that reflect the full variability of human movement.

To address these challenges, we introduced a Transformer-based deep learning model that uses a simple input—instantaneous speed—to achieve highly accurate transportation mode detection. We refer to this model as SPEEDTRANSFORMER. Using transportation mode classification as a case study, we demonstrate the model’s capability and versatility. Our contributions are threefold. First, we show that a Transformer-based neural network can achieve state-of-the-art performance using only speed as input. By leveraging positional encoding and multi-head attention, our model captured complex temporal patterns without elaborate feature engineering, thereby mitigating both privacy concerns and computational demands. Second, we demonstrate robust cross-regional generalizability through transfer learning: a model pre-trained on data primarily collected in Switzerland maintained exceptional performance when fine-tuned on samples from Beijing. Finally, we validated our approach

under real-world conditions by developing a novel smartphone mini-program and recruiting 348 participants for a one-month field experiment. The experimental results confirmed that our model’s advantages translated effectively from controlled environments to practical applications characterized by real-world uncertainty and variability.

2 Related Work

Transportation mode detection represents a central dimension of human mobility research, with downstream applications ranging from carbon footprint estimation [30] and tourism recommendations [31] to traffic management [32] and public health interventions [33]. With the proliferation of GPS-enabled devices and advances in machine learning, the field has undergone substantial progress in recent years, moving beyond traditional social scientific methods such as transportation surveys and adopting data-driven methodologies grounded in machine learning. Notable developments have emerged in both classical machine learning algorithms and deep learning approaches.

2.1 Machine Learning for Transportation Mode Detection and its Challenges

Classical machine learning (ML) algorithms formed the foundation of early data-driven approaches to transportation mode detection. These methods typically converted sequential GPS trajectories into statistical, tabular representations, with notable implementations including Decision Trees [34], Random Forests [35; 22], and Support Vector Machines [36]. Stenneth et al. [35] demonstrated the effectiveness of these models through systematic evaluation, while Jahangiri and Rakha [22] highlighted their versatility across different transportation modes, variations, and contexts. The logic underlying classical ML algorithms was conceptually similar to that of rule-based models, which relied on indicative features computed from GPS trajectories and used them to infer travel modes statistically. For example, mobility features derived from dense GPS trajectories—such as average speed and acceleration rate—were often effective in distinguishing between driving, walking, and cycling.

Although computationally efficient, these approaches depended heavily on domain expertise for feature engineering and performed poorly when handling variable-length inputs. In many inner-city trips, for instance, driving was only marginally faster than cycling, rendering average speed an unreliable discriminator. More advanced statistical features could improve performance but required specialized expertise and local contextual knowledge that were seldom available and sometimes unreliable.

Moreover, such methods posed risks to privacy and anonymity, as even a small number of precise and longitudinal GPS points could be sufficient to re-identify individuals [37]. Growing concerns regarding the collection, management, and disclosure of personal GPS data, together with advances in re-identification techniques, have further raised ethical issues surrounding GPS trajectory research [38; 39; 40]. In response, scholars and regulators have increasingly advocated for privacy-preserving techniques in mobility research—including applications such as transportation mode detection—as alternatives to classical machine learning approaches that depend on rich location features and extensive feature engineering [41; 42; 43; 44; 45].

Recurrent neural networks (RNNs), particularly Long Short-Term Memory (LSTM) networks [46], emerged as a dominant approach for transportation mode prediction due to their capacity to capture temporal dependencies in sequential data. Jiang et al. [47] pioneered the application of LSTMs for mobility analysis, and Asci and Guvensan [48] extended this work by incorporating attention mechanisms that improved performance across varied trip lengths. Hybrid architectures combining LSTMs with other neural components further advanced model accuracy—for example, the ConvLSTM model proposed by Nawaz et al. [49] leveraged convolutional layers for spatial feature extraction prior to temporal processing. Other innovations included Convolutional Neural Networks (CNNs) [50], autoregressive flow models [51], and semi-supervised learning approaches [52]. Despite these accuracy gains, such sophisticated architectures often required substantial computational resources and complex pre-processing to structure data according to model specifications, thereby limiting their practicality for real-world deployment [27].

2.2 Transformers for Mobility Modeling

Transformer architectures revolutionized sequence modeling through their reliance on self-attention and multi-head attention mechanisms [53; 21]. Models such as GPT-2 [54] and BERT [55] demonstrated exceptional performance on sequence-based data, significantly surpassing classical machine learning models in capturing complex sequential patterns. This success motivated researchers to explore whether Transformers’ superior capacity for modeling long-range dependencies could similarly advance mobility modeling, where understanding the relationships between distant points within a trajectory is critical [56].

Recent applications of Transformer architectures to mobility studies have shown promise, although the field remains in its early stages. For example, Hong et al. [57] incorporated Transformer components for next-location prediction while treating mode identification as a secondary task. Liang et al. [58] addressed challenges such as irregular spatiotemporal intervals but focused primarily on spatio-temporal dependencies rather than transportation mode prediction. More recently, Ribeiro et al. [59] achieved strong results using a vision Transformer approach [60], although their implementation required converting trajectories into image-based representations. Similarly, Drosouli et al. [61] converted GPS trajectory points into word tokens to apply the original BERT model [55], achieving notable results; however, this approach imposed a linguistic abstraction onto spatial data, making it less suitable for general-purpose mobility modeling.

Despite these advances, existing Transformer-based approaches for mobility modeling typically required extensive pre-processing, multiple input features, or auxiliary contextual information—making them computationally demanding and often impractical for real-world applications where only basic GPS data are available. Moreover, their generalizability across different geographical contexts has remained largely unexplored, as most evaluations have focused on performance within a single dataset rather than testing transferability between regions with distinct transportation infrastructures and mobility behaviors.

3 SpeedTransformer Architecture

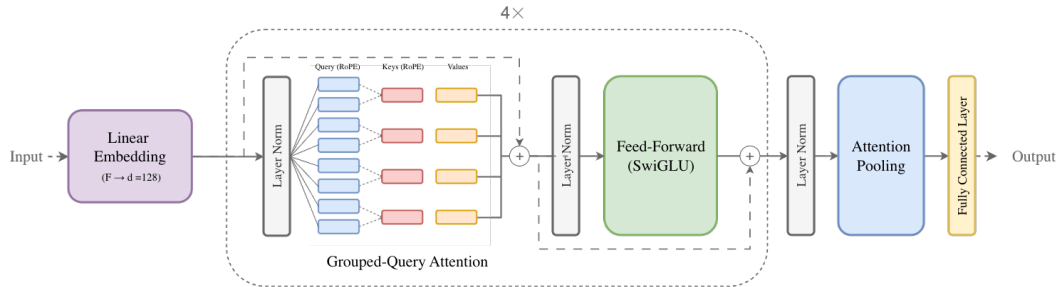


Figure 1: Transformer architecture

Our SPEEDTRANSFORMER architecture adapts the Transformer encoder framework proposed by Vaswani et al. [21], incorporating several key modifications to the data input, model structure, and output. First, the input sequences consist of instantaneous speeds computed from dense GPS trajectories collected via transportation applications on smartphones. These speed sequences are sampled at high frequencies—typically representing distances traveled over five to ten seconds—and therefore implicitly encoded higher-order motion features such as acceleration (the first derivative of speed) and jerk (the second derivative of speed). Given a complete speed sequence from trip start to end, each speed value serves as a token, which is subsequently embedded and transformed into a query vector representing its relationship to all other speed positions within the sequence.

Figure 1 illustrates the overall model architecture. Our model requires only raw scalar speed sequences as trajectory input. To accommodate variable input lengths, each trajectory is segmented into fixed-length sequences of $T = 200$ consecutive speed samples using a sliding window with a stride of 50 (see Appendix F for further discussion on window size selection). This segmentation is applied directly to the original speed sequences without temporal resampling, allowing the model to remain

robust to differences in sampling frequency across datasets.³ Shorter sequences are zero-padded, and a key-padding mask is applied to ensure that padded tokens are ignored during attention and pooling.

Each scalar speed value s_t is linearly projected into a $d = 128$ -dimensional embedding space (see Appendix D for details on the embedding process). The sequence of embedded speed vectors is then processed by a modified Transformer encoder. Owing to its attention mechanism, the model is able to extract sequential dependencies—such as acceleration and jerk—from these speed embeddings, which is critical for differentiating transportation modes. When trained on sufficiently large empirical datasets, the model effectively optimizes its capacity to detect transportation modes.

We replace the standard sinusoidal positional encoding with Rotary Positional Embeddings (RoPE), which is applied directly to the query (Q) and key (K) vectors in the attention mechanism [62]. RoPE encodes positional information through position-dependent rotations indexed by the sequence order, enabling the attention mechanism to model relative temporal dependencies in a continuous and rotation-invariant manner. This formulation is particularly well-suited for sequential mobility signals such as speed trajectories, where relative temporal structure is more informative than absolute position.

The encoder consists of $L = 4$ Pre-Norm Transformer blocks. Each block contains two key components: a Grouped-Query Attention (GQA) layer [63], which efficiently computes attention by grouping multiple query vectors per key-value pair, and a SwiGLU-activated feed-forward sublayer [64] that introduces non-linear transformations with improved gradient flow and expressivity (see Appendix E for a detailed explanation of SwiGLU). The computation within each block is expressed as follows:

$$\mathbf{z}_1 = \mathbf{x} + \text{Dropout}(\text{GQA}(\text{LayerNorm}(\mathbf{x}))), \quad (1)$$

$$\mathbf{z}_2 = \mathbf{z}_1 + \text{Dropout}(\text{FFN}_{\text{SwiGLU}}(\text{LayerNorm}(\mathbf{z}_1))), \quad (2)$$

Equation 1 describes the attention sub-layer, in which the input representation $\mathbf{x} \in \mathbb{R}^{T \times d}$ (a sequence of T tokens, each of dimension d) is first normalized using layer normalization before being passed to the GQA mechanism.

GQA divides the \mathbf{h} query heads into \mathbf{h}_{kv} groups, each group sharing a single key-value pair. This interpolates between multi-head and multi-query attention; using an intermediate number of groups retains much of the quality of multi-head attention while reducing memory and compute cost. We set $\mathbf{h} = 8$ query heads and $\mathbf{h}_{kv} = 4$ key/value heads in our experiments.

Equation 2 represents the feed-forward transformation that followed the attention mechanism. The intermediate output \mathbf{z}_1 is normalized again and passed through a SwiGLU-activated feed-forward network, $\text{FFN}_{\text{SwiGLU}}(\cdot)$, which introduces non-linear transformations to enhance representational capacity while maintaining computational efficiency.

Each layer applies layer normalization before both the attention and the feed-forward sub-layers and uses dropout on the sub-layer outputs before adding them back to the residual input, following the “residual dropout” strategy of the original Transformer

We employ $h = 8$ query heads and $h_{kv} = 4$ shared key/value heads, following the formulation of Ainslie et al. [63]. This design reduces both memory usage and computational cost by allowing multiple query heads to share the same key and value projections while preserving diversity across query subspaces. RoPE is applied to Q and K before computing scaled dot-product attention, and padding masks are introduced to ensure that zero-padded tokens did not contribute to the attention weights.

After the encoder stack, a final layer normalization is applied, producing the sequence representation $\mathbf{Z} = [\mathbf{z}_1, \dots, \mathbf{z}_T]$. The contextualized sequence is then aggregated through attention pooling. Specifically, each timestep embedding \mathbf{z}_t receives a learnable scalar attention score e_t , which is

³For the details of temporal sampling frequency, see Appendix L.

normalized using a masked softmax function across valid time-steps to obtain weights α_t :

$$e_t = \mathbf{w}_a^\top \mathbf{z}_t + b_a, \tag{3}$$

$$\alpha_t = \frac{\exp(e_t) \cdot M_t}{\sum_{\tau=1}^T \exp(e_\tau) \cdot M_\tau}, \tag{4}$$

where \mathbf{w}_a and b_a are learnable parameters, and $M_t \in \{0, 1\}$ is the mask for padding tokens. The pooled sequence embedding \mathbf{c} is computed as the weighted sum $\mathbf{c} = \sum_{t=1}^T \alpha_t \mathbf{z}_t$. Finally, after dropout regularization, \mathbf{c} is passed through a linear projection layer to produce the probability distribution $\hat{\mathbf{y}}$:

$$\hat{\mathbf{y}} = \text{softmax}(\mathbf{W}_c + \mathbf{b}_c), \tag{5}$$

where \mathbf{W}_c and \mathbf{b}_c represent the classifier weights and bias.

4 Datasets

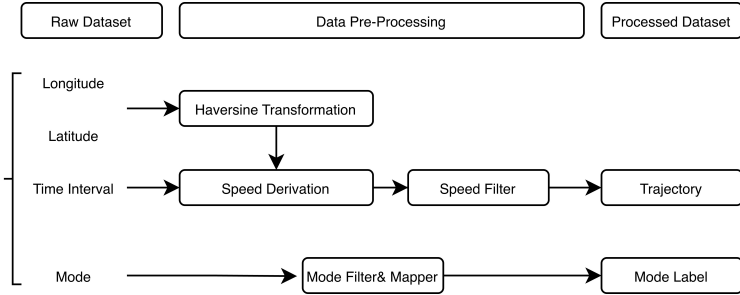


Figure 2: Data Pre-Processing

We utilized two longitudinal tracking datasets—the widely adopted Geolife dataset [26] and the Swiss MOBIS dataset [65]—which offered complementary strengths for evaluating our model. Summary statistics are presented in Table 1. As illustrated in Figure 2, we standardized their data structures through a unified pre-processing pipeline: we consolidated transportation modes into five consistent categories (Bike, Bus, Car, Train, Walk), unified the trajectory input format across datasets, excluded multi-model trajectories, converted geographic coordinates into speed sequences, removed abnormal trips with erroneous location data, and standardized transportation mode labels. Detailed descriptions of the pre-processing procedures and raw dataset statistics are provided in Appendix A.

4.1 MOBIS Dataset

The MOBIS dataset [14] was derived from an eight-week randomized controlled trial (RCT) on transport pricing involving 3,680 participants in Switzerland. Each participant used the *Catch-my-Day* mobile application (available for both iOS and Android), which continuously recorded GPS data via the device’s location services. The application captured daily travel patterns, storing raw trajectory data locally before uploading them to the MotionTag analytics platform, where trip segmentation and

Table 1: Comparison of MOBIS and Geolife Datasets

Mode	Data Points		Unique Trips	
	MOBIS	Geolife	MOBIS	Geolife
Bike	4,251,028	746,098	40,171	1,555
Bus	4,606,409	1,061,196	74,324	1,847
Car	88,965,473	627,047	542,078	1,293
Train	8,379,962	788,250	130,964	772
Walk	38,463,266	1,215,054	743,425	3,960
Total	144,666,138	4,437,645	1,530,962	9,427

transportation mode inference were performed. This extensive data collection process produced 255.3 million GPS records and 1.58 million labeled trips in the raw dataset. After applying our standardized pre-processing pipeline described in Appendix A, the resulting MOBIS dataset contained 144.7 million data points across 1.53 million unique trips distributed among five transportation modes, as summarized in Table 1.

4.2 Geolife Dataset

Geolife [26] was a widely used benchmark in transportation mode research, collected by Microsoft Research Asia from 182 users in Beijing over a five-year period (2007–2012). The dataset captured urban mobility through 17,000 trajectories covering approximately 1.2 million kilometers across Beijing’s complex transportation network. Data were recorded using various GPS loggers and GPS-enabled phones with different sampling rates, with 91% of trajectories collected at high density (every 1–5 seconds or every 5–10 meters). In addition to routine commutes, the Geolife dataset included leisure and sports activities such as shopping, sightseeing, and cycling, offering rich contextual diversity in trip purposes. After pre-processing to align with the MOBIS data structure, the Geolife dataset contained 4.44 million data points and 9,427 unique trips—substantially smaller than MOBIS, yet providing valuable geographical and temporal diversity for evaluating our model’s performance.

5 Experiments

We evaluated SPEEDTRANSFORMER under three experimental conditions. First, we benchmarked it against state-of-the-art transportation mode identification models on Geolife [26], enabling direct comparison with existing approaches. Second, we examined performance consistency across different geographical contexts by comparing it with classical LSTM baseline models on both the Swiss (MOBIS) [65] and Chinese (Geolife) datasets. Finally, we assessed cross-regional transferability through fine-tuning experiments, in which models pretrained on Swiss data were adapted to Chinese mobility patterns using small sample subsets.

5.1 Benchmarking Performance

To evaluate SpeedTransformer’s ability to achieve high accuracy with minimal input, we benchmarked against several state-of-the-art transportation mode identification models:

- **LSTM-Attention (Baseline)**: Our reconstructed baseline model implementing a classical bidirectional LSTM with attention mechanism [46]. This baseline is specifically designed to test whether pure attention-based mechanisms outperform recurrent networks augmented with attention, while maintaining the same minimal input requirement (speed only).
- **Deep-ViT** [59]: A Vision Transformer approach that transforms GPS features (speed, acceleration, bearing) into image representations using DeepInsight methodology before processing with a Vision Transformer architecture, combining traditional feature engineering with advanced deep learning.
- **CE-RCRF** [66]: A sequence-to-sequence framework (TaaS) that processes entire trajectories using a Convolutional Encoder to extract high-level features and a Recurrent Conditional Random Field to maintain contextual information at both feature and label levels, with specialized bus-related features to distinguish high-speed modes.
- **LSTM-based DNN** [67]: An ensemble of four LSTM networks that incorporates both time-domain trajectory attributes and frequency-domain statistics developed through discrete Fourier and wavelet transforms, creating a semi-supervised deep learning approach.
- **SECA** [52]: A Semi-supervised Convolutional Autoencoder that integrates a convolutional-deconvolutional autoencoder with a CNN classifier to simultaneously leverage labeled and unlabeled GPS segments, automatically extracting relevant features from 4-channel tensor representations.
- **ConvLSTM** [49]: A hybrid architecture that uses convolutional layers to extract spatial features from GPS data, followed by LSTM layers to capture temporal patterns, incorporating both location and weather features to enhance mode detection.

Table 2: Test Accuracy Comparison on Geolife (Ordered by Performance)

Model	Test Acc. (%)
SpeedTransformer (Ours)	95.97
Deep-ViT [59]	92.96
LSTM-based DNN [67]	92.70
LSTM-Attention (Baseline)	<u>92.40</u>
CE-RCRF [66]	85.23
SECA [52]	84.80
ConvLSTM [49]	83.81

All models were evaluated on the Geolife dataset using identical initial pre-processing and train-test splits. We have also added architectural comparison between our model and Transformer-based Deep-ViT in Appendix M. Table 2 presents the test accuracies ranked from highest to lowest.

SPEEDTRANSFORMER achieved the highest test accuracy of 95.97%, outperforming all competing approaches despite using only speed as input. Deep-ViT (92.96%) and the LSTM-based DNN (92.70%) achieved strong results but required more complex pre-processing or architectural components. Our LSTM-Attention baseline (92.40%) demonstrated that while recurrent networks with attention could capture temporal patterns effectively, they still lagged behind the pure attention-based design of SPEEDTRANSFORMER in predicting complex mobility patterns.

The lower-ranked models illustrated different architectural trade-offs. The CNN-ensemble extracted localized spatial patterns but struggled with sequential dependencies; ConvLSTM improved temporal modeling through its hybrid design but faced generalization challenges; and CE-RCRF treated trajectories as continuous sequences yet was hindered by architectural complexity. We also evaluated a simple rule-based model using the same process and found that it performed substantially worse than all machine learning models (Appendix H).

To further assess performance consistency across datasets, we compared SPEEDTRANSFORMER with our LSTM-Attention baseline on both the Geolife and MOBIS datasets. Figures 3 and 4 show that SPEEDTRANSFORMER not only converged faster and achieved higher validation accuracy but also maintained superior F1-scores across all transportation modes. The F1-score in Figure 4, which examines accuracy by class, provided a more granular and reliable measure of model performance under class imbalance. Moreover, Table 3 presents a detailed comparison of precision and recall between SPEEDTRANSFORMER and Deep-ViT—the most competitive alternative—demonstrating that SPEEDTRANSFORMER achieved a more balanced trade-off between precision and recall across datasets, underscoring its robustness and generalizability.

SPEEDTRANSFORMER demonstrated two significant advantages over the LSTM-Attention baseline: faster convergence and higher accuracy across both datasets. As shown in Figure 4, the model consistently achieved higher validation accuracies throughout training, reaching 94.22% accuracy on MOBIS compared to 92.33% for the LSTM-Attention model. The faster convergence was particularly valuable when working with large-scale mobility datasets such as MOBIS, where training efficiency was critical. We also observed that SPEEDTRANSFORMER achieved superior per-class F1-scores across all transportation modes in both the Geolife and MOBIS datasets. Class-wise error patterns are further summarized by the confusion matrices (Figure N6) and per-class F1 score (Figure N7) in Appendix N. Across different freezing strategies and experimental settings, SPEEDTRANSFORMER consistently outperforms the LSTM baseline, demonstrating robust performance, as shown in Tables C4, C5, C6, C7, and C8. Although the model required GPU resources, it remained relatively efficient, completing both training and inference on a single GPU node (Appendix I).

5.2 Cross-Regional Transferability

Learning from raw trajectories was feasible for all models, including rule-based approaches. However, deep learning architectures such as Transformers achieved state-of-the-art accuracy through inductive transfer and fine-tuning of pretrained models [68]. This transfer-learning approach was particularly advantageous when cross-regional differences in transportation networks and traffic dynamics pro-

Table 3: Validation Precision and Recall Comparison between Deep-ViT and SpeedTransformer on Geolife

Mode	Deep-ViT		SpeedTransformer	
	Precision (%)	Recall (%)	Precision (%)	Recall (%)
Walk	95.04	96.12	<u>96.72</u>	<u>99.90</u>
Bike	93.79	91.40	<u>98.54</u>	<u>95.45</u>
Bus	89.68	91.13	<u>98.14</u>	<u>95.49</u>
Car	<u>88.96</u>	87.26	<u>87.33</u>	<u>93.65</u>
Train	<u>90.00</u>	79.41	<u>95.66</u>	<u>92.93</u>
Macro Avg.	91.89	89.86	95.68	95.08

Table 4: Model Accuracy during Cross-Dataset Fine-Tuning from MOBIS to Small Geolife Subsets

Model	100 trips	200 trips
LSTM-Attention	75.47%	79.15%
SpeedTransformer	80.53%	86.13%

duced distinct patterns of transportation modes. To evaluate model transferability, we fine-tuned the MOBIS-pretrained models on small subsets of the Geolife dataset to simulate low-shot adaptation. Both SPEEDTRANSFORMER and LSTM-Attention were fine-tuned on 100 and 200 Geolife trips (approximately 1.1% and 2.2% of the dataset, respectively) for 20 epochs and were subsequently evaluated on the remaining samples. Table 4 reports the overall classification accuracy.

Fine-tuning followed a standardized low-shot protocol using MOBIS-pretrained checkpoints. For SPEEDTRANSFORMER, the encoder and attention layers were frozen, and training was performed with mixed precision for up to 20 epochs. The LSTM-Attention baseline was fine-tuned with smaller batch sizes, a lower learning rate, stronger regularization (dropout = 0.3, weight decay = 5e-3), and gradient clipping at 0.25. Hyperparameters were selected through a grid search to ensure optimal stability under limited supervision (see Appendix C). SPEEDTRANSFORMER achieved 80.53% accuracy with only 100 trips, surpassing LSTM-Attention by more than five percentage points, and further improved to 86.13% with 200 trips. These results confirmed its superior capacity to transfer learned mobility representations across regions with minimal labeled data.

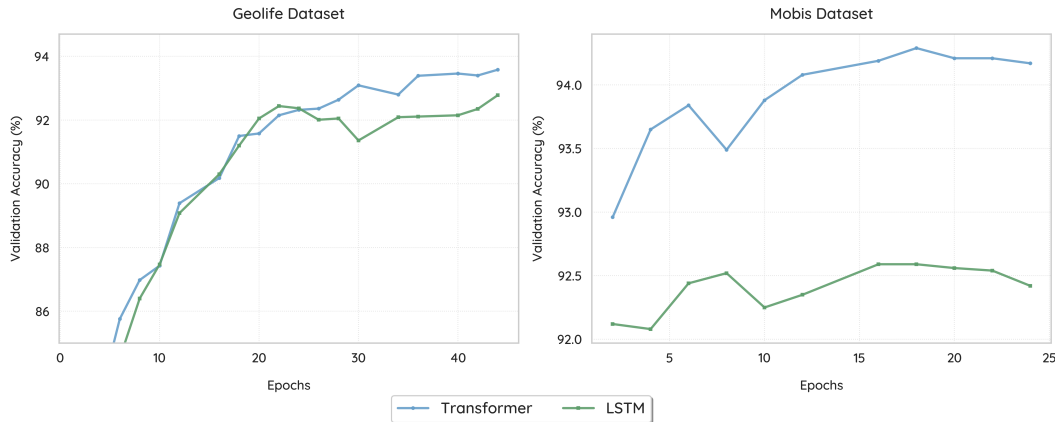


Figure 3: Validation accuracies over epochs for Geolife and MOBIS. The SpeedTransformer consistently converges faster and achieves higher overall accuracy than the LSTM-Attention baseline on both datasets.

6 Real-World Field Experiment

Having established SPEEDTRANSFORMER’s superior accuracy, minimal input requirements, and strong cross-regional transferability, we next evaluated its robustness under real-world conditions, where GPS data were inherently noisy, irregular, and device-dependent. While curated benchmarks provided clean and controlled comparisons, they did not capture the complexities of real-world mobility data, which were subject to signal loss, user heterogeneity, and hardware variability. To address this gap, we conducted a large-scale field experiment to assess SPEEDTRANSFORMER’s reliability in real-world environments characterized by high uncertainty and unpredictability.

6.1 Smartphone Application and Data Collection

We developed *CarbonClever*, a WeChat-integrated mini-program designed to estimate individual carbon footprints through continuous mobility tracking.⁴ The application provided a streamlined interface for trip initiation, real-time monitoring, and post-trip mode verification (Figure 5). A total of 348 participants from Jiangsu, China, were recruited through an environmental organization to record their daily movements.⁵

Real-world GPS traces differed substantially from those collected under laboratory conditions. The sampling frequencies varied widely: older iPhone SE models recorded locations every 30–60 s, whereas newer iPhone 14 Pro devices achieved 5–10 s intervals under identical conditions (see Appendix L for full temporal sampling comparison). As shown in Figure 6, trajectories exhibited irregular sampling densities, signal dropouts, and spurious positional jumps caused by multi-path effects or indoor transitions. Unlike benchmark datasets, we intentionally retained these imperfections to evaluate the model’s robustness under realistic deployment conditions.

6.2 Field Experiment Evaluation

We conducted a one-month field experiment from November 18, 2023 to December 23, 2024 that collected 649 verified trips totaling 108,823 GPS points from heterogeneous devices across both iOS and Android platforms, ensuring representative variability in sampling rates and noise profiles (see Appendix B for detailed data pre-processing). To assess real-world adaptability, we fine-tuned MOBIS-pretrained SpeedTransformer and LSTM-Attention models using progressively larger subsets

⁴A WeChat mini-program is a lightweight application embedded within the WeChat ecosystem. Functionally similar to a simplified smartphone app, the mini-program operates on top of the WeChat super-app, which is ubiquitously used in China. This integration enabled efficient participant recruitment and minimized testing costs across different mobile operating systems and device platforms.

⁵The experiment was approved by the Duke Kunshan University Institutional Review Board (protocol 2022CC073). See Appendix J for protocol summary.

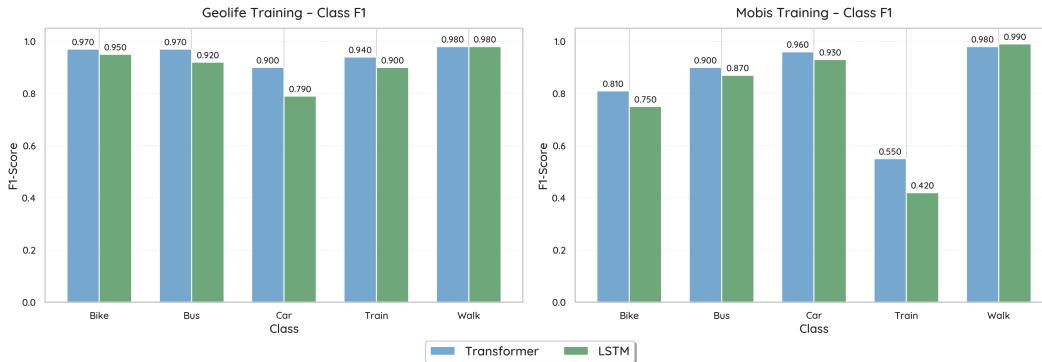


Figure 4: Per class F1-Score for Geolife and MOBIS trainings using SpeedTransformer and LSTM. The SpeedTransformer consistently achieves better results than the LSTM-Attention across all classes on both datasets.

Table 5: Summary of the Mini-Program Dataset

Mode	Number of Data Points	Number of Unique Trips
Walk	28,985	100
Bus	32,547	259
Car	40,885	205
Bike	4,901	36
Train	1,505	49
Total	108,823	649

Table 6: Fine-Tuning Accuracies of Models with Real-World Data Subsets (5-fold CV; mean \pm std, % accuracy)

Data Subset (%)	LSTM-Attention Acc. (%)	SpeedTransformer Acc. (%)
40% (251 trips)	88.79 \pm 2.15	90.27 \pm 2.04
50% (314 trips)	88.82 \pm 1.32	89.98 \pm 2.55
60% (377 trips)	89.34 \pm 1.86	90.40 \pm 2.17
70% (440 trips)	90.04 \pm 2.26	91.72 \pm 3.27
80% (502 trips)	89.30 \pm 2.52	90.11 \pm 4.54

of the collected data. Each model was trained for up to 20 epochs with early stopping and identical hyperparameter configurations derived from the grid search (Appendix C).

SpeedTransformer consistently outperformed the LSTM-Attention baseline across all real-world training subsets (Table 6). Results are reported using 5-fold cross-validation, with values shown as mean \pm standard deviation of accuracy across folds. SpeedTransformer achieved its best performance at the 70% subset (91.72 \pm 3.27%), while LSTM-Attention peaked at 90.04 \pm 2.26%. Overall, these real-world results reinforce our earlier findings: SpeedTransformer remains more accurate under genuine, noisy, and device-diverse GPS trajectories, helping bridge the gap between research prototypes and operational smart-mobility applications.

We also expanded our modeling experiments to include a per-class analysis, given that our field-experiment data are imbalanced and contain relatively few observations for bikes and trains. This imbalance negatively affected classification accuracy for these modes, resulting in accuracies below 0.8, as shown in Figure N7. Nevertheless, the per-class accuracies for bikes and trains still exceed 0.5, while the remaining classes maintain very high accuracies above 0.9.

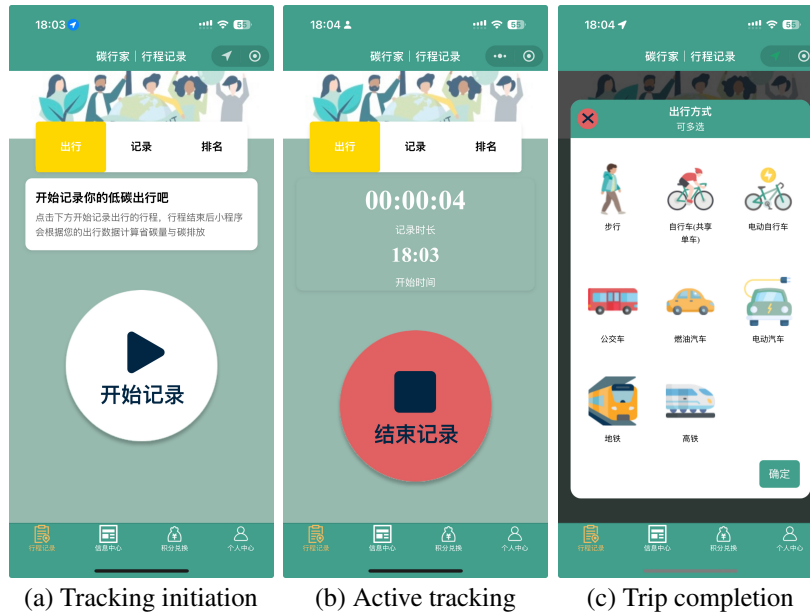


Figure 5: Trip tracking interface in the CarbonClever application: (a) Trip initiation screen, where users start a new trip recording. (b) Active tracking screen showing real-time trip duration and status. (c) Trip completion and mode confirmation screen, where users select and verify the transportation mode. All interface texts are originally in Chinese.

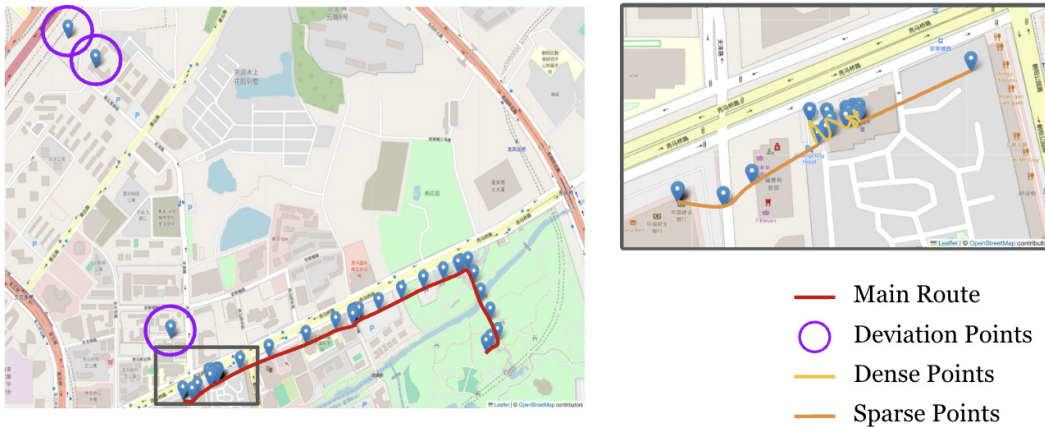


Figure 6: Example of real-world GPS trajectories. The red line indicates the main route, with varying point density reflecting heterogeneous sampling frequencies. Purple circles mark signal interference and positioning noise.

7 Discussion and Conclusion

Our research addressed three fundamental challenges in transportation mode detection: (1) the reliance on extensive feature engineering and input pre-processing, (2) limited model generalizability across distinct geographical contexts, and (3) insufficient and unpredictable real-world validation. By achieving state-of-the-art performance in transportation mode detection, our work demonstrated that Transformer-based neural network architectures, when coupled with high-quality training data, could substantially improve mode detection from GPS trajectories. More broadly, this approach had the potential to extract information from a wide range of mobility-based sequence data, and it contributed to a growing body of literature on transportation mode detection and its downstream applications in transportation research, GIS, urban analytics, and climate change science.

Compared to classical and deep ML methods [59; 66; 67; 52; 49], SPEEDTRANSFORMER outperformed feature-rich models despite using only speed as input. Across different hyperparameter configurations, our model consistently outperformed the LSTM-Attention baseline by 2–3% (Appendix C) and surpassed several other machine learning models by more than 10% (Table 2). It also outperformed the classical rule-based model, which relied solely on speed, by over 30% (Appendix H). This suggests that the Transformer-based model is highly effective at extracting useful information from dense speed sequences that would otherwise be underutilized, and it outperforms simpler deterministic models, classical machine-learning models, as well as other deep learning models.

The model’s strong performance was largely attributable to its attention mechanism (Appendix G). Nevertheless, our integration of SWIGLU activation, Grouped-Query Attention, and pre-attention Layer Normalization yielded modest yet consistent performance improvements, aligning with the findings of Shazeer [64] and Touvron et al. [69]. Consistent with Yu and Wang [70], our results further indicated that deeper neural network architectures were better suited to capturing the semantic and sequential structures embedded within GPS trajectories.

Moreover, this strong performance relied solely on instantaneous speed, without requiring GPS coordinates or additional engineered features. This architectural choice offered several advantages: it mitigates the direct exposure of sensitive location data by decoupling motion dynamics from absolute geographic coordinates [44; 37]. Specifically, we quantify this privacy benefit by contrasting the information entropy required to resolve a spatial position versus that of a speed observation. Because speed is a kinematic scalar inherently decoupled from raw geographic coordinates, it significantly limits the information available to a data-profiling adversary (for detailed discussion see Appendix K). In addition, using only speed as model input simplified preprocessing procedures, thereby enhancing reproducibility across various mobile devices and geographical contexts [71].

Furthermore, SPEEDTRANSFORMER exhibited strong cross-regional transferability. In the out-of-domain evaluation, it surpassed the LSTM-Attention model by 7% (Table 4), demonstrating robust generalizability across distinct geographical and transportation contexts—from Swiss transportation systems (MOBIS) to Chinese urban environment (Geolife). Travel behaviors varied substantially between these regions, and the two datasets were collected nearly a decade apart, introducing considerable differences in travel patterns across modes such as train, cycling, and automobile use. Remarkably, with only 100 fine-tuning trips, SPEEDTRANSFORMER achieved satisfactory accuracy (80.53%) on Geolife after pretraining on MOBIS. These findings suggested that SPEEDTRANSFORMER captured fundamental patterns of human mobility that persisted across infrastructural settings and regional mobility cultures.

Finally, to bridge the gap between research prototypes and real-world implementation, we validated SPEEDTRANSFORMER in a large-scale real-world experiment via our self-designed *CarbonClever* WeChat Mini-Program on personal smartphones. This mobile application collected GPS trajectories from 348 participants across diverse smartphones and operating systems in Jiangsu. This validation provides a third geographic context, representing mid-tier Asian cities that differ significantly in infrastructural scale and traffic dynamics from the European (MOBIS) and megacity (Geolife) environments. This dataset included unpredictable real-world conditions, irregular sampling intervals, signal interferences and device-specific noises. SPEEDTRANSFORMER consistently outperformed the LSTM-Attention baseline across all fine-tuning results, achieving 94.22% accuracy with 50% of the real-world training data, compared to 87.57% for LSTM-Attention. While accuracy decreased

slightly due to data irregularities, SPEEDTRANSFORMER retained high stability across transportation modes, confirming its robustness for practical deployment.

A key limitation of Transformer-based models, including SPEEDTRANSFORMER, was their sensitivity to training data quality. As shown in Table 3 and Figure 4, the model performed less effectively for the *Train* class in the MOBIS dataset, where data imbalance and under-representation reduced its ability to generalize. As Van Hulse et al. [72] noted, class imbalance posed significant challenges to ML accuracy. Still, by pretraining on the larger, more balanced MOBIS dataset and fine-tuning on the smaller, imbalanced Geolife subsets, SPEEDTRANSFORMER maintained strong predictive accuracy with minimal performance degradation under distributional shift. The model performed even better using our real-world experimental data, achieving an accuracy of 89.12% with just 94 training trips, compared to 86.13% in the Geolife fine-tuning task using 200 training trips (Table 6). These results underscored the model’s adaptability to data-sparse and heterogeneous mobility environments. These results underscored the model’s adaptability to data-sparse and heterogeneous mobility environments.

In addition, despite the privacy advantages of speed-only inputs, the approach is not entirely immune to sophisticated privacy attacks. Although our model avoids collecting raw coordinates, sequential speed profiles can, in some cases, inadvertently reveal identifiable behavioral patterns [73].⁶ If an adversary possesses extensive side-channel information, such as high-resolution traffic flow databases or signal timing schedules, they could theoretically attempt to match a specific speed profile to a known corridor, potentially inferring coarse-grained route information. Future work can investigate the integration of enhanced techniques, such as differential privacy and federated learning, to provide formal guarantees against such attacks.

We also conducted a targeted failure analysis (Appendix O) focusing on the *Train* class, whose accuracy is notably lower than that of other classes. In MOBIS, the train category encompasses multiple train modes—such as underground subway, tram, and metro-style services—and is sometimes intermixed with trajectories that resemble car or bus travel. As a result, the associated speed profiles become difficult to separate. These findings suggest that either more sophisticated models or additional mode-specific training data may be needed to further improve classification performance.

Finally, the inherent opacity of the Transformer architecture poses a limitation regarding its interpretability—specifically the difficulty of attributing learned patterns to interpretable mobility features such as acceleration bursts, stop durations, or route choices. Future research could investigate hybrid architectures that integrate Transformer attention mechanisms with physically interpretable mobility features and extend the framework to incorporate contextual signals—such as weather, traffic density, and land use—for downstream mobility tasks, including origin–destination flow estimation and route-level analysis. In addition, expanding evaluation to regions with different road infrastructures and behavioral norms could further validate model universality.

The original datasets of MOBIS and Geolife can be found at their respective project websites: the MOBIS dataset (<https://www.research-collection.ethz.ch/handle/20.500.11850/553990>) and the Geolife dataset (<https://www.microsoft.com/en-us/research/publication/Geolife-gps-trajectory-dataset-user-guide/>), both accessible on May 26, 2025.

Acknowledgments

We thank the Institute for Transport Planning and Systems at ETH Zürich for providing the data used in our model training. We are also grateful to Yucen Xiao, Peilin He, Zhixuan Lu, Yili Wen, Shanheng Gu, Ziyue Zhong, and Ni Zheng for their excellent research assistance. This project was supported by the 2024 Kunshan Municipal Key R&D Program under the Science and Technology Special Project (No. KS2477). ChatGPT 5 was used solely for grammar checking. All remaining errors are our own.

Disclosure statement

No potential conflict of interest was reported by the author(s).

⁶In our real-world experiment, however, all participants lived in dense urban areas, where individual speed profiles were effectively unrecognizable among hundreds of thousands of co-residents.

Data and codes availability statement

Replication data and code can be found at: <https://github.com/othmaneehc/SpeedTransformer>. The repository provides source code for data processing, model training and evaluation.

We have also prepared two Colab notebooks: one with the main results and most appendix results at <https://shorturl.at/dzVkb>, and another with the remaining appendix results at <https://shorturl.at/XZcB8>.

The original datasets of MOBIS and Geolife can be found at their respective project websites: the MOBIS dataset (<https://www.research-collection.ethz.ch/handle/20.500.11850/553990>) and the Geolife dataset (<https://www.microsoft.com/en-us/research/publication/Geolife-gps-trajectory-dataset-user-guide/>), both accessed on May 26, 2025.

Additional information

Funding

This project was supported by the 2024 Kunshan Municipal Key R&D Program under the Science and Technology Special Project (No. KS2477).

Notes on contributors

Yuandong Zhang

Yuandong Zhang is a master's student in Computer Science at the University of California, San Diego, USA. His research interests include deep learning and generative AI. He contributed to conceptualisation, methodology, software, validation, and writing – original draft.

Othmane Echchabi

Othmane Echchabi is a master's student in Computer Science affiliated with Mila – Quebec AI Institute and McGill University, Canada. His research focuses on deep learning and spatial image processing. He contributed to conceptualisation, methodology, software, validation, and writing – original draft.

Tianshu Feng

Tianshu Feng is a master's student in Data Science at the University of Pennsylvania, USA. His interests include data engineering and experimental workflows for machine learning. He contributed to software, data curation, and writing – review & editing.

Wenyi Zhang

Wenyi Zhang is an undergraduate student at Duke Kunshan University, China. Her interests include data processing and applied machine learning. She contributed to software and data curation.

Hsuai-Kai Liao

Hsuai-Kai Liao is an undergraduate student at Duke Kunshan University, China. His interests include data science and computational experimentation. He contributed to software and validation.

Charles Chang

Charles Chang is an Assistant Professor of Environment and Urban Studies at Duke Kunshan University, China. His research focuses on computational social science, geospatial analysis, and deep learning applications. He contributed to conceptualisation, supervision, funding acquisition, and writing – review & editing.

References

- [1] Marta C Gonzalez, Cesar A Hidalgo, and Albert-Laszlo Barabasi. Understanding individual human mobility patterns. *nature*, 453(7196):779–782, 2008.
- [2] Nadine Schuessler and Kay W Axhausen. Processing raw data from global positioning systems without additional information. *Transportation Research Record*, 2105(1):28–36, 2009.
- [3] Zhenxing Yao, Yu Zhong, Qiang Liao, Jie Wu, Haode Liu, and Fei Yang. Understanding human activity and urban mobility patterns from massive cellphone data: Platform design and applications. *IEEE Intelligent Transportation Systems Magazine*, 13(3):206–219, 2020.
- [4] Shih-Lung Shaw, Ming-Hsiang Tsou, and Xinyue Ye. Human dynamics in the mobile and big data era. *International Journal of Geographical Information Science*, 30(9):1687–1693, 2016.
- [5] Giovanni Bonaccorsi, Francesco Pierri, Matteo Cinelli, Andrea Flori, Alessandro Galeazzi, Francesco Porcelli, Ana Lucia Schmidt, Carlo Michele Valensise, Antonio Scala, Walter Quattrociocchi, et al. Economic and social consequences of human mobility restrictions under covid-19. *Proceedings of the national academy of sciences*, 117(27):15530–15535, 2020.
- [6] Celia McMichael. Human mobility, climate change, and health: Unpacking the connections. *The Lancet Planetary Health*, 4(6):e217–e218, 2020.
- [7] Hugo Barbosa, Surendra Hazarie, Brian Dickinson, Aleix Bassolas, Adam Frank, Henry Kautz, Adam Sadilek, José J Ramasco, and Gourab Ghoshal. Uncovering the socioeconomic facets of human mobility. *Scientific reports*, 11(1):8616, 2021.
- [8] Matthew Zook, Menno-Jan Kraak, and Rein Ahas. Geographies of mobility: applications of location-based data. *International Journal of Geographical Information Science*, 29(11):1935–1940, 2015. doi: 10.1080/13658816.2015.1061667. URL <https://doi.org/10.1080/13658816.2015.1061667>.
- [9] Bin Guo, Zhu Wang, Zhiwen Yu, Yu Wang, Neil Y Yen, Runhe Huang, and Xingshe Zhou. Mobile crowd sensing and computing: The review of an emerging human-powered sensing paradigm. *ACM computing surveys (CSUR)*, 48(1):1–31, 2015.
- [10] Yaguang Tao, Alan Both, and Matt Duckham. Analytics of movement through checkpoints. *International Journal of Geographical Information Science*, 32(7):1282–1303, 2018.
- [11] Bastien Girod, Detlef P van Vuuren, and Bert de Vries. Influence of travel behavior on global co2 emissions. *Transportation Research Part A: Policy and Practice*, 50:183–197, 2013.
- [12] Mehrdad Tajalli and Ali Hajbabaie. On the relationships between commuting mode choice and public health. *Journal of Transport & Health*, 4:267–277, 2017.
- [13] Zijia Wang, Feng Chen, and Taku Fujiyama. Carbon emission from urban passenger transportation in beijing. *Transportation Research Part D: Transport and Environment*, 41:217–227, 2015.
- [14] Joseph Molloy, Alberto Castro, Thomas Götschi, Beaumont Schoeman, Christopher Tcherenkov, Uros Tomic, Beat Hintermann, and Kay W. Axhausen. The MOBIS dataset: a large GPS dataset of mobility behaviour in Switzerland. *Transportation*, 50(5):1983–2007, October 2023. ISSN 1572-9435. doi: 10.1007/s11116-022-10299-4. URL <https://doi.org/10.1007/s11116-022-10299-4>.
- [15] Daniel Preotiuc-Pietro and Trevor Cohn. Mining user behaviours: A study of check-in patterns in location based social networks. In *Proceedings of the 3rd Annual ACM Web Science Conference (WebSci 2013)*, 2013. doi: 10.1145/2464464.2464479.
- [16] Jason B. Gordon, Harilaos N. Koutsopoulos, Nigel H. M. Wilson, and John P. Attanucci. Automated inference of linked transit journeys in london using fare-transaction and vehicle location data. *Transportation Research Record*, 2343:17 – 24, 2013. URL <https://api.semanticscholar.org/CorpusID:109903480>.

- [17] Xin Lu, Linus Bengtsson, and Petter Holme. Predictability of population displacement after the 2010 haiti earthquake. *Proceedings of the National Academy of Sciences*, 109(29):11576–11581, 2012.
- [18] H. Barbosa, F. B. de Lima-Neto, A. Evsukoff, et al. The effect of recency to human mobility. *EPJ Data Science*, 4:21, 2015. doi: 10.1140/epjds/s13688-015-0059-8. URL <https://doi.org/10.1140/epjds/s13688-015-0059-8>.
- [19] Michael F Goodchild. The quality of big (geo) data. *Dialogues in Human Geography*, 3(3): 280–284, 2013.
- [20] Luca Pappalardo, Ed Manley, Vedran Sekara, and Laura Alessandretti. Future directions in human mobility science. *Nature Computational Science*, 3(7):588–600, 2023. ISSN 2662-8457. doi: 10.1038/s43588-023-00469-4. URL <https://doi.org/10.1038/s43588-023-00469-4>.
- [21] Ashish Vaswani, Noam Shazeer, Niki Parmar, Jakob Uszkoreit, Llion Jones, Aidan N. Gomez, Lukasz Kaiser, and Illia Polosukhin. Attention is all you need. *arXiv preprint arXiv:1706.03762*, 2017. doi: 10.48550/arXiv.1706.03762. URL <http://arxiv.org/abs/1706.03762>.
- [22] Arash Jahangiri and Hesham A. Rakha. Applying Machine Learning Techniques to Transportation Mode Recognition Using Mobile Phone Sensor Data. *IEEE Transactions on Intelligent Transportation Systems*, 16(5):2406–2417, October 2015. ISSN 1558-0016. doi: 10.1109/TITS.2015.2405759. URL <https://ieeexplore.ieee.org/document/7063936>. Conference Name: IEEE Transactions on Intelligent Transportation Systems.
- [23] Fengli Xu, Zhen Tu, Yong Li, Pengyu Zhang, Xiaoming Fu, and Depeng Jin. Trajectory recovery from ash: User privacy is not preserved in aggregated mobility data. In *Proceedings of the 26th international conference on world wide web*, pages 1241–1250, 2017. doi: <https://doi.org/10.1145/3038912.3052620>.
- [24] M. Rzeszewski and P. Luczys. Care, indifference and anxiety—attitudes toward location data in everyday life. *ISPRS International Journal of Geo-Information*, 7(10):383, 2018. doi: 10.3390/ijgi7100383. URL <https://doi.org/10.3390/ijgi7100383>.
- [25] Ziliang Zhao, Shih-Lung Shaw, Yang Xu, Feng Lu, Jie Chen, and Ling Yin. Understanding the bias of call detail records in human mobility research. *International Journal of Geographical Information Science*, 30(9):1738–1762, 2016. doi: 10.1080/13658816.2015.1137298. URL <https://doi.org/10.1080/13658816.2015.1137298>.
- [26] Yu Zheng, Xing Xie, and Wei-Ying Ma. GeoLife: A collaborative social networking service among user, location and trajectory. *IEEE Data Eng. Bull.*, 33(2):32–39, 2010. URL <https://citeseerx.ist.psu.edu/document?repid=rep1&type=pdf&doi=24ccdcba118ff9a72de4840efb848c7c852ef247>. Publisher: Citeseer.
- [27] Anita Graser, Anahid Jalali, Jasmin Lampert, Axel Weißenfeld, and Krzysztof Janowicz. MobilityDL: A review of deep learning from trajectory data. *arXiv preprint arXiv:2402.00732*, 2024. doi: 10.48550/arXiv.2402.00732. URL <http://arxiv.org/abs/2402.00732>. Submitted to Geoinformatica.
- [28] Paul A. Zandbergen. Accuracy of iphone locations: A comparison of assisted gps, wifi and cellular positioning. *Transactions in GIS*, 13:5–25, 2009. doi: 10.1111/j.1467-9671.2009.01152.x. URL <https://doi.org/10.1111/j.1467-9671.2009.01152.x>.
- [29] Y. J. Cui and S. S. Ge. Autonomous vehicle positioning with gps in urban canyon environments. In *Proceedings 2001 ICRA. IEEE International Conference on Robotics and Automation (Cat. No.01CH37164)*, volume 2, pages 1105–1110, 2001. doi: 10.1109/ROBOT.2001.932759.
- [30] V. Manzoni, D. Manilo, K. Kloeckl, and C. Ratti. Transportation mode identification and real-time co2 emission estimation using smartphones: How co2go works - technical report. Technical report, SENSEable City Lab, Massachusetts Institute of Technology and Politecnico di Milano, 2010. URL <http://senseable.mit.edu/co2go/images/co2go-technical-report.pdf>.

- [31] XueFei Xiao, ChunHua Li, XingJie Wang, and AnPing Zeng. Personalized tourism recommendation model based on temporal multilayer sequential neural network. *Scientific Reports*, 15(1):382, 2025. doi: 10.1038/s41598-024-84581-z. URL <https://doi.org/10.1038/s41598-024-84581-z>.
- [32] Adrian C. Prelicean, Gyözö Gidófalvi, and Yusak O. Susilo. Transportation mode detection – an in-depth review of applicability and reliability. *Transport Reviews*, 37(4):442–464, 2016. doi: 10.1080/01441647.2016.1246489.
- [33] A. Aleta, D. Martín-Corral, M. A. Bakker, A. Pastore Y Piontti, M. Ajelli, M. Litvinova, M. Chinazzi, N. E. Dean, M. E. Halloran, I. M. Jr Longini, A. Pentland, A. Vespignani, Y. Moreno, and E. Moro. Quantifying the importance and location of sars-cov-2 transmission events in large metropolitan areas. *Proceedings of the National Academy of Sciences of the United States of America*, 119(26):e2112182119, 2022. doi: 10.1073/pnas.2112182119. URL <https://doi.org/10.1073/pnas.2112182119>.
- [34] Yu Zheng, Quannan Li, Yukun Chen, Xing Xie, and Wei-Ying Ma. Understanding mobility based on GPS data. In *Proceedings of the 10th international conference on Ubiquitous computing*, pages 312–321, Seoul Korea, September 2008. ACM. ISBN 978-1-60558-136-1. doi: 10.1145/1409635.1409677. URL <https://dl.acm.org/doi/10.1145/1409635.1409677>.
- [35] Leon Stenneth, Ouri Wolfson, Philip S. Yu, and Bo Xu. Transportation mode detection using mobile phones and GIS information. In *Proceedings of the 19th ACM SIGSPATIAL International Conference on Advances in Geographic Information Systems*, pages 54–63, Chicago Illinois, November 2011. ACM. ISBN 978-1-4503-1031-4. doi: 10.1145/2093973.2093982. URL <https://dl.acm.org/doi/10.1145/2093973.2093982>.
- [36] Adel Bolbol, Tao Cheng, Ioannis Tsapakis, and James Haworth. Inferring hybrid transportation modes from sparse GPS data using a moving window SVM classification. *Computers, Environment and Urban Systems*, 36(6):526–537, November 2012. ISSN 0198-9715. doi: 10.1016/j.compenvurbsys.2012.06.001. URL <https://www.sciencedirect.com/science/article/pii/S0198971512000543>.
- [37] Yves-Alexandre De Montjoye, César A Hidalgo, Michel Verleysen, and Vincent D Blondel. Unique in the crowd: The privacy bounds of human mobility. *Scientific reports*, 3(1):1376, 2013.
- [38] Katina Michael, Andrew McNamee, and Michael G Michael. The emerging ethics of human-centric gps tracking and monitoring. In *2006 International Conference on Mobile Business*, pages 34–34. IEEE, 2006.
- [39] Predrag Klasnja, Sunny Consolvo, Tanzeem Choudhury, Richard Beckwith, and Jeffrey Hightower. Exploring privacy concerns about personal sensing. In *International Conference on Pervasive Computing*, pages 176–183. Springer, 2009.
- [40] Robert P Minch. Privacy issues in location-aware mobile devices. In *37th Annual Hawaii International Conference on System Sciences, 2004. Proceedings of the*, pages 10–pp. IEEE, 2004.
- [41] Grace Ng-Kruelle, Paul A Swatman, Douglas S Rebne, and J Felix Hampe. The price of convenience: Privacy and mobile commerce. *Quarterly journal of electronic commerce*, 3: 273–286, 2002.
- [42] John Krumm. A survey of computational location privacy. *Personal and Ubiquitous Computing*, 13(6):391–399, 2009.
- [43] Kang G Shin, Xiaoen Ju, Zhigang Chen, and Xin Hu. Privacy protection for users of location-based services. *IEEE Wireless Communications*, 19(1):30–39, 2012.
- [44] Stuart A Thompson and Charlie Warzel. Twelve million phones, one dataset, zero privacy. In *Ethics of data and analytics*, pages 161–169. Auerbach Publications, 2022.

- [45] Hongbo Jiang, Jie Li, Ping Zhao, Fanzi Zeng, Zhu Xiao, and Arun Iyengar. Location privacy-preserving mechanisms in location-based services: A comprehensive survey. *ACM Computing Surveys (CSUR)*, 54(1):1–36, 2021.
- [46] Sepp Hochreiter and Jürgen Schmidhuber. Long Short-Term Memory. *Neural Comput.*, 9(8):1735–1780, November 1997. ISSN 0899-7667. doi: 10.1162/neco.1997.9.8.1735. URL <https://doi.org/10.1162/neco.1997.9.8.1735>.
- [47] Xiang Jiang, Erico N. de Souza, Ahmad Pesaraghader, Baifan Hu, Daniel L. Silver, and Stan Matwin. TrajectoryNet: An embedded GPS trajectory representation for point-based classification using recurrent neural networks. *arXiv preprint arXiv:1705.02636*, 2017. doi: 10.48550/arXiv.1705.02636. URL <http://arxiv.org/abs/1705.02636>.
- [48] Guven Asci and M. Amac Guvensan. A novel input set for LSTM-based transport mode detection. In *2019 IEEE International Conference on Pervasive Computing and Communications Workshops (PerCom Workshops)*, pages 107–112. IEEE, 2019. doi: 10.1109/PERCOMW.2019.8730799. URL <https://ieeexplore.ieee.org/abstract/document/8730799>.
- [49] Asif Nawaz, Huang Zhiqiu, Wang Senzhang, Yasir Hussain, Izhar Khan, and Zaheer Khan. Convolutional LSTM based transportation mode learning from raw GPS trajectories. *IET Intelligent Transport Systems*, 14(6):570–577, 2020. ISSN 1751-9578. doi: 10.1049/iet-its.2019.0017. URL <https://onlinelibrary.wiley.com/doi/abs/10.1049/iet-its.2019.0017>. _eprint: <https://onlinelibrary.wiley.com/doi/pdf/10.1049/iet-its.2019.0017>.
- [50] Sina Dabiri and Kevin Heaslip. Inferring transportation modes from GPS trajectories using a convolutional neural network. *Transportation Research Part C: Emerging Technologies*, 86:360–371, January 2018. ISSN 0968-090X. doi: 10.1016/j.trc.2017.11.021. URL <https://www.sciencedirect.com/science/article/pii/S0968090X17303509>.
- [51] Sumanto Dutta and Bidyut Kr. Patra. Inferencing transportation mode using unsupervised deep learning approach exploiting GPS point-level characteristics. *Applied Intelligence*, 53(10):12489–12503, May 2023. ISSN 1573-7497. doi: 10.1007/s10489-022-04140-9. URL <https://doi.org/10.1007/s10489-022-04140-9>.
- [52] Sina Dabiri, Chang-Tien Lu, Kevin Healip, and Chandan K. Reddy. Semi-Supervised Deep Learning Approach for Transportation Mode Identification Using GPS Trajectory Data. *IEEE Transactions on Knowledge and Data Engineering*, 32(5):1010–1023, May 2020. ISSN 1041-4347, 1558-2191, 2326-3865. doi: 10.1109/TKDE.2019.2896985. URL <https://ieeexplore.ieee.org/document/8632766/>.
- [53] Jianpeng Cheng, Li Dong, and Mirella Lapata. Long short-term memory-networks for machine reading. *arXiv preprint arXiv:1601.06733*, 2016.
- [54] Alec Radford, Jeff Wu, Rewon Child, David Luan, Dario Amodei, and Ilya Sutskever. Language models are unsupervised multitask learners. 2019.
- [55] Jacob Devlin, Ming-Wei Chang, Kenton Lee, and Kristina Toutanova. BERT: Pre-training of deep bidirectional transformers for language understanding. In Jill Burstein, Christy Doran, and Thamar Solorio, editors, *Proceedings of the 2019 Conference of the North American Chapter of the Association for Computational Linguistics: Human Language Technologies, Volume 1 (Long and Short Papers)*, pages 4171–4186, Minneapolis, Minnesota, June 2019. Association for Computational Linguistics. doi: 10.18653/v1/N19-1423. URL <https://aclanthology.org/N19-1423/>.
- [56] Hao Xue, Bhanu Prakash Voutharoja, and Flora D. Salim. Leveraging language foundation models for human mobility forecasting. In *Proceedings of the 30th International Conference on Advances in Geographic Information Systems, SIGSPATIAL '22*, New York, NY, USA, 2022. Association for Computing Machinery. ISBN 9781450395298. doi: 10.1145/3557915.3561026. URL <https://doi.org/10.1145/3557915.3561026>.
- [57] Ye Hong, Henry Martin, and Martin Raubal. How do you go where? Improving next location prediction by learning travel mode information using transformers. In *Proceedings of the 30th International Conference on Advances in Geographic Information Systems*, pages 1–10,

- November 2022. doi: 10.1145/3557915.3560996. URL <http://arxiv.org/abs/2210.04095>. arXiv:2210.04095 [cs].
- [58] Yuxuan Liang, Kun Ouyang, Yiwei Wang, Xu Liu, Hongyang Chen, Junbo Zhang, Yu Zheng, and Roger Zimmermann. TrajFormer: Efficient trajectory classification with transformers. In *Proceedings of the 31st ACM International Conference on Information & Knowledge Management*, CIKM '22, pages 1229–1237, New York, NY, USA, 2022. Association for Computing Machinery. ISBN 9781450392365. doi: 10.1145/3511808.3557481.
- [59] Ricardo Ribeiro, Alina Trifan, and António J. R. Neves. A deep learning approach for transportation mode identification using a transformation of GPS trajectory data features into an image representation. *International Journal of Data Science and Analytics*, February 2024. ISSN 2364-4168. doi: 10.1007/s41060-024-00510-3. URL <https://doi.org/10.1007/s41060-024-00510-3>.
- [60] Alexey Dosovitskiy, Lucas Beyer, Alexander Kolesnikov, Dirk Weissenborn, Xiaohua Zhai, Thomas Unterthiner, Mostafa Dehghani, Matthias Minderer, Georg Heigold, Sylvain Gelly, Jakob Uszkoreit, and Neil Houlsby. An image is worth 16x16 words: Transformers for image recognition at scale. *arXiv preprint arXiv:2010.11929*, 2021. doi: 10.48550/arXiv.2010.11929. URL <http://arxiv.org/abs/2010.11929>. ICLR 2021.
- [61] Ifigenia Drosouli, Athanasios Voulodimos, Paris Mastorocostas, Georgios Miaoulis, and Djamchid Ghazanfarpour. Tmd-bert: a transformer-based model for transportation mode detection. *Electronics*, 12(3):581, 2023.
- [62] Jianlin Su, Yu Lu, Shengfeng Pan, Ahmed Murtadha, Bo Wen, and Yunfeng Liu. Roformer: Enhanced transformer with rotary position embedding. *arXiv preprint arXiv:2104.09864*, 2021. doi: 10.48550/arXiv.2104.09864. URL <https://arxiv.org/abs/2104.09864>.
- [63] Joshua Ainslie, James Lee-Thorp, Michiel de Jong, Yury Zemlyanskiy, Federico Lebrón, and Sumit Sanghai. Gqa: Training generalized multi-query transformer models from multi-head checkpoints. *arXiv preprint arXiv:2305.13245*, 2023. doi: 10.48550/arXiv.2305.13245. URL <https://arxiv.org/abs/2305.13245>.
- [64] Noam Shazeer. Glu variants improve transformer. *arXiv preprint arXiv:2002.05202*, 2020. doi: 10.48550/arXiv.2002.05202. URL <https://arxiv.org/abs/2002.05202>.
- [65] Daniel Heimgartner and Kay W Axhausen. Modal splits before, during, and after the pandemic in switzerland. *Transportation research record*, 2678(7):1084–1099, 2024.
- [66] Jiaqi Zeng, Yi Yu, Yong Chen, Di Yang, Lei Zhang, and Dianhai Wang. Trajectory-as-a-sequence: A novel travel mode identification framework. *Transportation Research Part C: Emerging Technologies*, 146:103957, 2023. ISSN 0968-090X. doi: 10.1016/j.trc.2022.103957. URL <https://www.sciencedirect.com/science/article/pii/S0968090X22003709>.
- [67] James J. Q. Yu. Semi-supervised deep ensemble learning for travel mode identification. *Transportation Research Part C: Emerging Technologies*, 112:120–135, March 2020. ISSN 0968-090X. doi: 10.1016/j.trc.2020.01.003. URL <https://www.sciencedirect.com/science/article/pii/S0968090X19309416>.
- [68] Jeremy Howard and Sebastian Ruder. Universal language model fine-tuning for text classification. *arXiv preprint arXiv:1801.06146*, 2018.
- [69] Hugo Touvron, Thibaut Lavril, Gautier Izacard, Xavier Martinet, Marie-Anne Lachaux, Timothée Lacroix, Baptiste Rozière, Naman Goyal, Eric Hambro, Faisal Azhar, et al. Llama: Open and efficient foundation language models. *arXiv preprint arXiv:2302.13971*, 2023.
- [70] Wenhao Yu and Guanwen Wang. Graph based embedding learning of trajectory data for transportation mode recognition by fusing sequence and dependency relations. *International Journal of Geographical Information Science*, 37(12):2514–2537, 2023.
- [71] Adel Bolbol, Tao Cheng, Ioannis Tsapakis, and James Haworth. Inferring hybrid transportation modes from sparse gps data using a moving window svm classification. *Computers, Environment and Urban Systems*, 36(6):526–537, 2012.

- [72] Jason Van Hulse, Taghi M Khoshgoftaar, and Amri Napolitano. Experimental perspectives on learning from imbalanced data. In *Proceedings of the 24th international conference on Machine learning*, pages 935–942, 2007.
- [73] Aliaksei Lareshyn, Kalle Åström, and Karin Brundell-Freij. From speed profile data to analysis of behaviour: classification by pattern recognition techniques. *IATSS research*, 33(2):88–98, 2009.
- [74] Haosheng Huang, Yi Cheng, and Robert Weibel. Transport mode detection based on mobile phone network data: A systematic review. *Transportation Research Part C: Emerging Technologies*, 101:297–312, 2019.
- [75] Latanya Sweeney. k-anonymity: a model for protecting privacy. *Int. J. Uncertain. Fuzziness Knowl.-Based Syst.*, 10(5):557–570, October 2002. ISSN 0218-4885. doi: 10.1142/S0218488502001648. URL <https://doi.org/10.1142/S0218488502001648>.

A Data Pre-Processing

Our pre-processing pipeline transformed raw GPS trajectories from both the Geolife and MOBIS datasets into standardized, analysis-ready data suitable for model training. The process involved several key steps:

Data Consolidation: For Geolife, we first converted the original PLT files into CSV format, while MOBIS data was already structured appropriately. Tables A2 and A3 show the initial distribution of transportation modes in the raw datasets.

Distance Calculation: We computed distances between consecutive GPS points using the Haversine formula, which accounts for Earth’s curvature:

$$d = 2r \cdot \arcsin \left(\sqrt{\sin^2 \left(\frac{\phi_2 - \phi_1}{2} \right) + \cos(\phi_1) \cos(\phi_2) \sin^2 \left(\frac{\lambda_2 - \lambda_1}{2} \right)} \right) \quad (6)$$

where ϕ represents latitude, λ represents longitude (both in radians), and r is Earth’s radius (6,371,000 meters).

Speed Derivation: We computed speeds by dividing the distance by the time difference between consecutive points, converting to km/h:

$$v = \frac{d}{\Delta t} \cdot 3.6 \quad (7)$$

Label Standardization: We harmonized transportation mode labels across datasets, consolidating similar modes (e.g., merging ‘taxi’ with ‘car’, and ‘subway’ with ‘train’) to create consistent categories across datasets.

Mode-Specific Filtering: We applied speed thresholds for each transportation mode (Table A1) to remove physically implausible values caused by GPS errors or data anomalies.

Trip Quality Control: We removed trips with fewer than three GPS points, as these would depart from real world scenarios and they provide insufficient sequential information for the model to learn meaningful patterns.

This pre-processing reduced the original datasets to five standardized transportation modes (Bike, Bus, Car, Train, and Walk) suitable for cross-dataset modeling. The final datasets used for model training and evaluation contained 144.7 million data points across 1.53 million trips from MOBIS and 4.44 million data points across 9,427 trips from Geolife, as detailed in Table 1.

Table A1: Speed Thresholds for Each Mode

Mode	Min Speed (km/h)	Max Speed (km/h)
Bike	0.5	50
Bus	1.0	120
Car	3.0	180
Train	3.0	350
Walk	0.1	15

B GPS Tracking on Smartphone Application

Our smartphone application, *CarbonClever* WeChat Mini-Program, implements real-time GPS tracking to collect high-quality mobility data while minimizing battery consumption. When a participant initiates tracking, the application activates the device’s location services using a dynamic sampling strategy designed to balance data density and energy efficiency.

The location tracking module periodically queries the device’s location sensors at intervals ranging from 10 to 30 seconds, depending on device capability and movement speed. Although the application can technically record location data at one-second intervals, a sampling rate of 10–30 seconds effectively preserves the accuracy of speed estimation while preventing excessive battery drain on users’ smartphones.

Table A2: Summary of the MOBIS Dataset

Mode	Number of Data Points	Number of Unique Trips
Aerialway	109	7
Airplane	718,156	3,185
Bicycle	6,568,587	41,166
Bus	7,450,378	77,361
Car	160,348,026	553,259
Ferry	228	12
LightRail	5,824,637	39,657
RegionalTrain	3,674,625	22,413
Subway	425,223	6,917
Train	10,166,760	34,064
Tram	3,591,472	32,428
Walk	56,539,324	767,923
Total	255,307,525	1,578,392

Table A3: Summary of the Labeled Geolife Dataset

Mode	Number of Data Points	Number of Unique Trips
Airplane	9,196	14
Bike	951,350	1,555
Boat	3,565	7
Bus	1,271,062	1,851
Car	512,939	782
Motorcycle	336	2
Run	1,975	4
Subway	309,699	613
Taxi	241,404	513
Train	556,397	177
Walk	1,582,693	3,991
Total	5,440,616	9,509

Each recorded sample captures the user’s current geographic coordinates (ϕ, λ) and timestamp (t) . As new coordinates are received, the application computes the great-circle distance between consecutive points using the Haversine formula (8):

$$d = 2r \arcsin \left(\sqrt{\sin^2 \left(\frac{\phi_2 - \phi_1}{2} \right) + \cos(\phi_1) \cos(\phi_2) \sin^2 \left(\frac{\lambda_2 - \lambda_1}{2} \right)} \right), \quad (8)$$

where d denotes the great-circle distance in meters, r is Earth’s radius (6,371,000 meters), and ϕ_1 , λ_1 , ϕ_2 , and λ_2 are the latitudes and longitudes (in radians) of consecutive GPS points. The average speed between two points is then calculated as:

$$v = \frac{d}{\Delta t}, \quad (A2)$$

where Δt represents the elapsed time (in seconds) between successive samples. This real-time computation allows for efficient on-device speed estimation while maintaining privacy, since only scalar speed values—not precise location traces—are required for model input.

These calculations are performed in real time within the application’s frontend, allowing users to receive immediate feedback on their trip statistics. Simultaneously, the raw coordinate data, computed speeds, distances, and timestamps are securely transmitted to a cloud database via encrypted API

calls. This cloud infrastructure also hosts our pre-trained SpeedTransformer and LSTM-Attention models, enabling real-time transportation mode prediction.

During our experiments, the application’s tracking module collected GPS trajectories from a diverse range of smartphone devices and operating systems. Table 5 summarizes the dataset collected through the mini-program, which exhibits natural variations in sampling frequency and signal quality—characteristics typical of real-world usage. This authentic dataset proved invaluable for validating the SpeedTransformer model under conditions that closely mirror practical deployment environments.

C Full Grid Hyper-Parameter Space Search Results & Analysis

Experimental reporting conventions. The following tables enumerate all training and fine-tuning runs conducted in this experiment. To improve readability, we omit dataset size and run identifiers, and instead report the complete set of hyper-parameters that uniquely define each configuration. Unless otherwise specified, all accuracies correspond to the test split (%).

Column definitions. *LR*, *BS*, *DO*, *WD*, *Ep.*, and *Early* denote learning rate, batch size, dropout, weight decay, maximum epochs, and early-stopping patience, respectively. For the LSTM-Attention model, additional columns include *Hidden* (hidden state dimension) and *Layers* (number of stacked LSTM layers). For the SpeedTransformer, columns include *Heads* (attention heads), *d_{model}* (embedding dimension), *KV Heads* (shared key/value heads when using grouped-query attention), *Warmup* (number of warmup steps), and *Freeze Policy* (which modules were frozen or reinitialized). In fine-tuning tables, *Subset (%)* indicates the percentage of the target training data used (e.g., 15%, 20%, etc.).

Summary of results. Tables C4, C5, C6, C7, C8, C9, C10, and C11 report the results. Across all training and fine-tuning experiments, SpeedTransformer consistently achieved higher accuracy and stronger cross-domain generalization than the LSTM-Attention baseline, particularly under limited-data and transfer learning. When trained directly on the Geolife and MOBIS datasets, both models converged to high accuracy (approximately 93–96%). However, notable differences emerged in transfer learning and fine-tuning scenarios.

For in-domain training, SpeedTransformer exhibited optimal performance with a learning rate of 2×10^{-4} , batch size of 512, dropout of 0.1, and embedding dimension $d_{model} = 128$ with 8 attention heads. Accuracy reached 95.97% on Geolife and 94.22% on MOBIS, with stability across modest parameter variations, suggesting strong generalization capacity without overfitting. LSTM-Attention achieved comparable accuracy (around 92.7%) using a learning rate of 1×10^{-3} , hidden dimension 128–256, and two recurrent layers, but its performance was more sensitive to learning rate changes.

In cross-dataset transfer (MOBIS \rightarrow Geolife), fine-tuned SpeedTransformer models surpassed 85% test accuracy under optimal configurations, while LSTM-Attention plateaued around 84%. Among transformer variants, the best results were obtained when the last block was reinitialized (85.7%) or when no layers were frozen (84.2%). By contrast, freezing attention or feed-forward layers caused performance to drop below 65%, confirming that full end-to-end adaptation is necessary for effective transfer across mobility domains.

Fine-tuning from transfer data (MOBIS \rightarrow Real-World App Experiment) further demonstrated the efficiency of the transformer architecture. Even when using only 15% of the experiment dataset, SpeedTransformer achieved 89.1% accuracy, outperforming LSTM-Attention (86.6%) under comparable settings. As the fine-tuning subset increased, SpeedTransformer’s accuracy scaled up smoothly, reaching 94.2% with 50% of the target data. Embedding-freezing strategies yielded intermediate performance (up to 87.8%), while partial freezing or warmup schedules offered no clear benefit. These results indicate that SpeedTransformer effectively leverages prior mobility representations with minimal data, whereas LSTM-Attention requires larger sample sizes to reach similar accuracy.

Overall, the experiments reveal three consistent patterns. First, moderate learning rates ($2\text{--}5 \times 10^{-4}$) and full-layer fine-tuning yield the most robust convergence across datasets. Second, SpeedTransformer’s attention-based representations exhibit superior transferability and resilience to dataset heterogeneity compared with recurrent encoders, shown in Figure N7. Third, increasing the fine-tuning subset improves performance approximately monotonically, suggesting that the pre-trained

Table C4: Summary of LSTM–Attention performance trained on MOBIS. All runs use Ep.=50, WD=1e-4, EarlyStop=7, unless noted.

Configuration	LR	Batch Size	Dropout	Hidden Units	Layers	Accuracy (%)
Base (best)	1×10^{-3}	128	0.1	128	2	92.40
Smaller batch	1×10^{-3}	64	0.1	128	2	92.20
Higher dropout	1×10^{-3}	64	0.2	128	2	92.15
Deeper network	1×10^{-3}	64	0.1	128	3	92.26
Larger hidden size	1×10^{-3}	64	0.1	256	2	92.04
Higher learning rate	2×10^{-3}	64	0.1	128	2	92.14
Lower learning rate	5×10^{-4}	128	0.1	256	3	92.33
Smaller batch, lower LR	5×10^{-4}	64	0.1	128	2	92.35

Table C5: Summary of SpeedTransformer performance trained on MOBIS. All runs use Ep.=50, WD=1e-4, EarlyStop=7.

Configuration	LR	Batch Size	Dropout	d_model	Heads / KV Heads	Accuracy (%)
Base (best)	1×10^{-4}	512	0.1	128	8 / 4	94.22
Higher LR	2×10^{-4}	512	0.1	128	8 / 2	94.20
Larger model	2×10^{-4}	512	0.1	192	12 / 6	93.71
Larger embedding	2×10^{-4}	512	0.1	256	8 / 4	93.54
Smaller batch	2×10^{-4}	1024	0.1	128	8 / 4	93.69
Higher dropout	2×10^{-4}	512	0.2	128	8 / 4	93.54
Higher LR	3×10^{-4}	512	0.1	128	8 / 4	94.09

mobility embeddings capture domain-invariant movement structures that generalize across tracking environments.

D Input Embeddings

Each scalar speed value s_t is linearly projected into a $d_{model} = 128$ -dimensional embedding space, producing an input embedding matrix $\mathbf{E} \in \mathbb{R}^{T \times d_{model}}$. This projection enables the model to represent one-dimensional scalar speeds within a high-dimensional latent space suitable for Transformer-based sequence modeling:

$$\mathbf{e}_t = \mathbf{W}_e s_t + \mathbf{b}_e, \quad (9)$$

where s_t denotes the scalar speed at time step t , $\mathbf{W}_e \in \mathbb{R}^{1 \times d}$ is the learnable weight matrix, and $\mathbf{b}_e \in \mathbb{R}^d$ is the learnable bias vector. The resulting embeddings $\mathbf{E} = [\mathbf{e}_1, \mathbf{e}_2, \dots, \mathbf{e}_T]$ serve as the model’s input sequence to subsequent positional encoding and self-attention layers.

E SwiGLU Activation

Each feed-forward subnetwork adopts the SwiGLU activation [64], defined as:

$$\text{SwiGLU}(\mathbf{x}) = (\mathbf{x}\mathbf{W}_1) \odot \text{Swish}(\mathbf{x}\mathbf{W}_2)\mathbf{W}_3, \quad (10)$$

where \odot denotes element-wise multiplication, $\mathbf{W}_1, \mathbf{W}_2, \mathbf{W}_3$ are learnable weight matrices, and $\text{Swish}(\mathbf{x}) = \mathbf{x}\sigma(\mathbf{x})$ with $\sigma(\cdot)$ being the sigmoid activation function. SwiGLU enhances representational expressivity and improves training stability relative to standard ReLU-based feed-forward layers.

Table C6: Summary of LSTM–Attention performance trained on Geolife. All runs use Ep.=50, WD=1e-4, EarlyStop=7, unless noted.

Configuration	LR	Batch Size	Dropout	Hidden Units	Layers	Accuracy (%)
Base (best)	1×10^{-3}	128	0.1	128	2	92.77
Smaller batch	1×10^{-3}	64	0.1	128	2	91.77
Higher dropout	1×10^{-3}	64	0.2	128	2	92.71
Deeper network	1×10^{-3}	64	0.1	128	3	92.16
Larger hidden size	1×10^{-3}	64	0.1	256	2	92.73
Higher learning rate	2×10^{-3}	64	0.1	128	2	92.56
Lower learning rate	5×10^{-4}	128	0.1	256	3	92.40
Smaller batch, lower LR	5×10^{-4}	64	0.1	128	2	91.63

Table C7: Summary of SpeedTransformer performance trained on Geolife. All models use Ep.=50, WD=1e-4, EarlyStop=7, unless noted.

Configuration	Learning Rate (LR)	Model Size (d_{model})	Attention Heads (Q/KV)	Accuracy (%)
Base (optimal)	2×10^{-4}	128	8 / 4	95.97
Reduced KV heads	2×10^{-4}	128	8 / 2	95.36
Larger model	2×10^{-4}	192	12 / 6	94.72
Larger embedding	2×10^{-4}	256	8 / 4	94.69
Higher LR	3×10^{-4}	128	8 / 4	94.68
Lower LR	1×10^{-4}	128	8 / 4	94.44
Higher batch size	2×10^{-4}	128	8 / 4	92.72
Higher dropout	2×10^{-4}	128	8 / 4	92.70

F Model Window Size

Figure F1 supports our choice of $T = 200$, showing that performance improves steadily with larger window sizes up to 200, beyond which accuracy plateaus and slightly declines. The 500-sample configuration also required a reduced batch size due to GPU memory constraints, potentially impacting training stability. Overall, $T = 200$ represents the optimal size between accuracy, computational efficiency, and training stability, capturing sufficient motion dynamics without introducing unnecessary redundancy or overfitting.

G SpeedTransformer in Original Transformer Model Architecture

We also conduct experiments using the original Transformer architecture, proposed by Vaswani et al. [21], for a comparison. Although the core architecture shares the transformer encoder backbone with the final model presented in Section 3, this initial version employed sinusoidal positional encodings and a standard feed-forward block instead of Rotary Positional Embeddings (RoPE) and SwiGLU activations. The updated design described in the main text improved both training stability, computational efficiency, and cross-dataset transferability.

The following subsections summarize the original architecture, input encoding strategy, and optimization setup for the model. We provide experiment results, which serves as a reference for ablation comparisons.

The model architecture adapts the transformer encoder framework [21]. Figure G2 presents the overall architecture of our model. To incorporate sequential order information, we add sinusoidal positional encoding to these embeddings, shown in Equation 11.

$$\mathbf{PE}(pos, 2i) = \sin\left(\frac{pos}{10000^{2i/d_{\text{model}}}}\right), \quad \mathbf{PE}(pos, 2i + 1) = \cos\left(\frac{pos}{10000^{2i/d_{\text{model}}}}\right) \quad (11)$$

Table C8: Summary of fine-tuning LSTM-Attention (MOBIS \rightarrow Geolife). All models use BS=128, DO=0.3, WD=1e-4, Ep.=60, and EarlyStop=7.

Learning Rate (LR)	Hidden Size	Accuracy (%)	Notes
1×10^{-3}	64–256	84.17	Optimal configuration
5×10^{-4}	64–256	84.13	Comparable to best
1×10^{-4}	64–256	82.84	Slight underfitting
5×10^{-5}	—	75.47–79.15	Low performance (few epochs)

Table C9: Summary of fine-tuning SpeedTransformer (MOBIS \rightarrow Geolife). All models use BS=512, WD=1e-4, DO=0.2, Ep.=50, and EarlyStop=7.

Learning Rate (LR)	Best Freeze Policy	Warmup Steps	Accuracy (%)
5×10^{-5}	Reinit last block	0	85.07
1×10^{-4}	Reinit last block	0	85.70
2×10^{-4}	Attention frozen	0	86.38
2×10^{-4}	Reinit last block	0	86.30
1×10^{-4}	Embeddings frozen	0	84.22
1×10^{-4}	None (all trainable)	0	84.08
2×10^{-4}	None (all trainable)	0	85.01
5×10^{-5} to 2×10^{-4}	Any freeze w/ warmup (100–500)	—	63–67 (no gain)

where pos is the position in the sequence, i is the dimension index, and d_{model} is the embedding dimension.

We use the same 200 variable-length sliding window, in consistent with the main model. We projects scalar speed value into high-dimensional vector representations through linear transformation followed by non-linear activation in Equation 12.

$$\mathbf{E} = \text{ReLU}(\mathbf{W}_e \cdot \mathbf{S} + \mathbf{b}_e) \quad (12)$$

where \mathbf{S} represents input speed values and \mathbf{E} the resulting embeddings.

These encoding enables the model to differentiate positions and captures temporal variations that are critical to distinguish transportation modes over time. For example, information such as acceleration patterns can be inferred from sequences of trajectories.

After the positional encoding, the inputs are fed into a self-attention layer, which helps the encoder to check speed at other positions in the input sequence as it encodes a speed at a specific location, as shown in Figure G3. Vaswani et al. [21] established that attention mechanisms compute weighted aggregations of value vectors where weights are determined by compatibility scores between query and key vectors, which we adopt the scaled dot-product attention formulation as defined in Equation (1) of Vaswani et al. (2017) and use their definition of scaled dot-product attention in Equation 13.

$$\text{Attention}(\mathbf{Q}, \mathbf{K}, \mathbf{V}) = \text{softmax}\left(\frac{\mathbf{Q}\mathbf{K}^\top}{\sqrt{d_k}}\right)\mathbf{V} \quad (13)$$

In this formulation, \mathbf{Q} represents queries that seek information, \mathbf{K} encodes keys that store information, and \mathbf{V} contains values that are aggregated according to query-key compatibility. For self-attention, all three matrices derive from the same input sequence, which enables each position to attend to all positions within the sequence.

The multi-head attention mechanism extends this concept by computing attention in parallel across different representation subspaces. We follow Vaswani et al. [21] and use their definition of multihead

Table C10: Summary of LSTM-Attention fine-tuning results from MOBIS \rightarrow Real-World App Experiment. All runs use 50 epochs, EarlyStop with patience = 10 (Pat. 10), dropout = 0.3, and weight decay = 1e-4.

Subset (%)	LR	Hidden Units	Batch Size	Early Stop	Pat.	Accuracy (%)
15	5×10^{-4}	128	128	10	Pat.10	86.62
20	5×10^{-4}	128	128	10	Pat.10	88.02
30	5×10^{-4}	128	128	10	Pat.10	88.97
40	5×10^{-4}	128	128	10	Pat.10	87.45
50	5×10^{-4}	128	128	10	Pat.10	87.57
15	1×10^{-3}	128–256	128	10	Pat.10	86.19
15	1×10^{-4}	128–256	128	10	Pat.10	85.18

Table C11: Summary of SpeedTransformer fine-tuning results from MOBIS \rightarrow Real-World App Experiment. All runs used 50 epochs, EarlyStop with patience = 10 (Pat. 10), dropout = 0.2, and weight decay = 1e-4.

Subset (%)	Learning Rate	Warmup Steps	Freeze Policy	Batch Size	Early Stop	Accuracy (%)
15	5×10^{-4}	0	None	512	Pat.10	89.12
20	5×10^{-4}	0	None	512	Pat.10	82.53
30	5×10^{-4}	0	None	512	Pat.10	<u>91.15</u>
40	5×10^{-4}	0	None	512	Pat.10	88.78
50	5×10^{-4}	0	None	512	Pat.10	94.22
15	1×10^{-4}	0–100	Attention/Embedding frozen	512	Pat.10	69.3–72.9
15	2×10^{-4}	0–100	Embeddings frozen	512	Pat.10	71.6–80.6
15	5×10^{-4}	0–100	Embeddings frozen	512	Pat.10	77.2–87.8

representation in Equation 15.

$$\text{MultiHead}(\mathbf{Q}, \mathbf{K}, \mathbf{V}) = \text{Concat}(\text{head}_1, \dots, \text{head}_h) \mathbf{W}^O \quad (14)$$

$$\text{head}_i = \text{Attention}(\mathbf{Q} \mathbf{W}_i^Q, \mathbf{K} \mathbf{W}_i^K, \mathbf{V} \mathbf{W}_i^V) \quad (15)$$

Here, \mathbf{W}_i^Q , \mathbf{W}_i^K , and \mathbf{W}_i^V are learned projection matrices that transform the original embeddings into different subspaces, while \mathbf{W}^O projects the concatenated outputs back to the model dimension.

In line with standard deep learning practice, each encoder layer includes a position-wise feed-forward network (FFN) applied independently to every position. The input to the FFN is formed by summing the token embeddings and positional encodings, as shown in Equation 16:

$$\mathbf{z} = \mathbf{x} + \mathbf{PE}, \quad (16)$$

where \mathbf{x} denotes the token embedding and \mathbf{PE} represents the positional encoding.

Table F12: Test accuracy and loss across different window sizes (Geolife dataset).

W. Size	Test Acc. (%)	Test Loss	Run Name
20	77.58	0.5778	Geolife_ws20_lr2e-4_bs512_h8_d128_kv4_do0.1
50	84.86	0.4043	Geolife_ws50_lr2e-4_bs512_h8_d128_kv4_do0.1
100	92.07	0.2600	Geolife_ws100_lr2e-4_bs512_h8_d128_kv4_do0.1
200	95.97	0.1525	Geolife_ws200_lr2e-4_bs512_h8_d128_kv4_do0.1
300	95.04	0.1753	Geolife_ws300_lr2e-4_bs512_h8_d128_kv4_do0.1
400	94.53	0.1703	Geolife_ws400_lr2e-4_bs256_h8_d128_kv4_do0.1
500	95.03	0.1800	Geolife_ws500_lr2e-4_bs256_h8_d128_kv4_do0.1

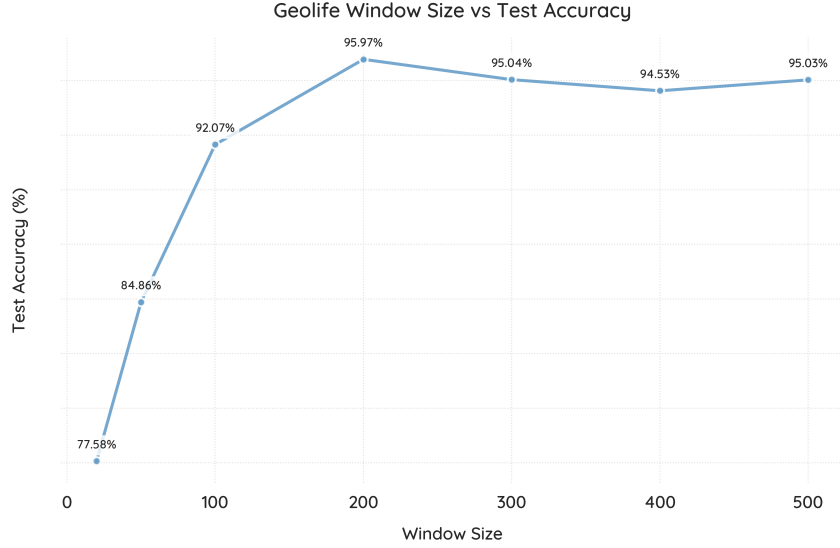


Figure F1: Effect of window size on test accuracy for the Geolife dataset. A window size of 200 provides the optimal balance between temporal context and computational efficiency, achieving the highest accuracy (95.97%).

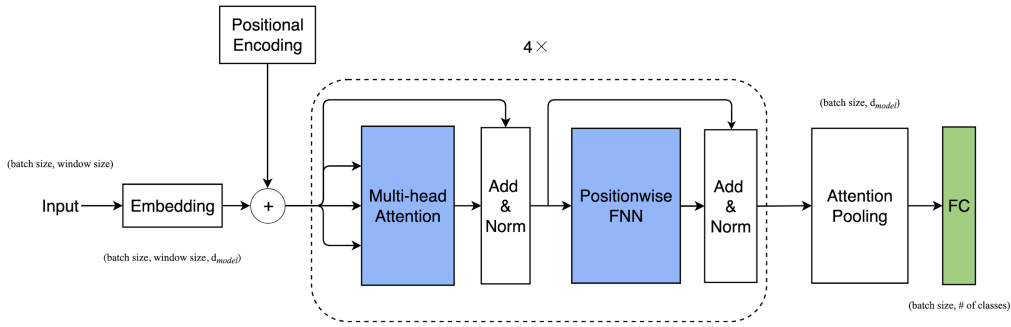


Figure G2: Transformer architecture for transportation mode classification.

Residual connections and layer normalization are applied around each sub-layer to facilitate gradient flow and enhance training stability. To generate a fixed-length representation from variable-length sequences, we employ attention-based pooling. The position-aware input \mathbf{z} is then passed into the feed-forward network (FFN), defined in Equation 17:

$$\text{FFN}(\mathbf{x} + \mathbf{PE}) = \max(0, (\mathbf{x} + \mathbf{PE})\mathbf{W}_1 + \mathbf{b}_1)\mathbf{W}_2 + \mathbf{b}_2, \quad (17)$$

where \mathbf{W}_1 and \mathbf{W}_2 are weight matrices, and \mathbf{b}_1 and \mathbf{b}_2 are bias terms. To incorporate sequential order information, token embeddings are first augmented with sinusoidal positional encoding through the attention mechanism and softmax normalization. These position-aware inputs are then processed by the FFN in Equation 17, enabling the model to capture complex non-linear transformations of input representations at each position.

The model is trained using the cross-entropy loss function, which quantifies the divergence between the predicted and ground-truth transportation modes, as shown in Equation 18:

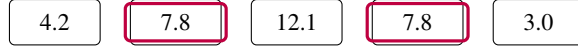
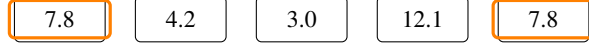
Trajectory A (5 Hz samples)**Trajectory B (same speeds, different order)**

Figure G3: Two GPS speed sequences share the same multiset of speeds but in different orders. Without position information the embeddings for repeated values (e.g., 7.8 m/s) are identical. With positional encoding we form $\mathbf{z}_t = E(v_t) + P(t)$, allowing attention to model order-dependent patterns.

$$\mathcal{L} = - \sum_{i=1}^N \sum_{c=1}^C y_{i,c} \log(p_{i,c}), \quad (18)$$

where N is the number of samples, C is the number of classes, $y_{i,c} \in \{0, 1\}$ denotes the ground-truth label (1 if sample i belongs to class c), and $p_{i,c}$ is the predicted probability of class c for sample i .

Final classification is performed through a linear projection of the pooled representation, followed by a softmax activation to generate a probability distribution over transportation modes, as defined in Equation 19:

$$p(y = c \mid \mathbf{c}) = \frac{\exp(\mathbf{w}_c^\top \mathbf{c} + b_c)}{\sum_{j=1}^C \exp(\mathbf{w}_j^\top \mathbf{c} + b_j)}, \quad (19)$$

where \mathbf{c} denotes the pooled feature vector, and \mathbf{w}_c and b_c represent the weight vector and bias term for class c , respectively.

We implement AdamW optimization with weight decay, learning rate scheduling, dropout regularization, and gradient clipping. This architecture enables efficient discovery of complex temporal patterns in speed data, capturing the distinctive signatures of different transportation modes without requiring additional input features or pre-processing steps.

Table G13: Per-class accuracy (recall) of LSTM and Transformer models across datasets. Each model was trained on Geolife and MOBIS, and fine-tuned from MOBIS to Geolife and Mini-Program datasets.

Model	Training Setup	Bike	Bus	Car	Train	Walk
LSTM	Geolife	0.92	0.86	0.86	0.92	0.99
	MOBIS	0.61	0.84	0.99	0.28	0.99
	MOBIS \rightarrow Geolife	0.59	0.84	0.57	0.79	0.72
	MOBIS \rightarrow Mini-Program	0.39	0.69	0.93	0.79	0.86
Transformer	Geolife	0.93	0.96	0.92	0.87	0.99
	MOBIS	0.78	0.88	0.98	0.43	0.99
	MOBIS \rightarrow Geolife	0.75	0.88	0.75	0.80	0.99
	MOBIS \rightarrow Mini-Program	0.40	0.70	1.00	0.43	0.99

As shown in Table G13, the Transformer consistently outperforms the LSTM across all datasets and transfer setups, confirming its superior ability to capture temporal dependencies and generalize across domains.

H Rule-based Model

Several prior studies on transportation mode detection rely on simple rule-based models built on handcrafted heuristics derived from dense GPS trajectory data [74]. Such models typically depend on a small number of summary statistics (e.g., speed percentiles, stop ratios, or acceleration variability), require no auxiliary GIS data, and are computationally inexpensive. However, their performance is highly sensitive to threshold choices and to behavioral heterogeneity across users, cities, and datasets.

To establish a strong heuristic baseline, we implemented a hierarchical rule-based classifier operating on sliding windows of raw GPS trajectories. Unlike earlier implementations that rely exclusively on fixed expert-defined thresholds, we calibrated the rule parameters separately for each dataset using the training split, yielding dataset-specific but still purely heuristic decision rules. The rules operate as follows. First, the 95th-percentile speed within each window is used to separate low-speed modes (walk, bike) from motorized and rail modes. Second, windows exceeding a high-speed threshold are classified as rail. Finally, among remaining motorized windows, the stop ratio and acceleration variability are used to distinguish buses from cars.

Table H14 summarizes the calibrated thresholds used in our experiments. All speed values are expressed in meters per second (m/s).

Rule	Threshold (m/s)	Description / Condition for Mode Assignment
walk_p95_max	≤ 3.0	Windows with 95th-percentile speed below 3.0 m/s are classified as <i>walk</i> .
bike_p95_max	≤ 8.0	Windows with 95th-percentile speed between 3.0–8.0 m/s are classified as <i>bike</i> .
road_p95_min	≥ 17.4 (18.0*)	Windows exceeding this threshold are treated as motorized road transport (<i>bus</i> or <i>car</i>).
rail_p95_min	≥ 27.5 (40.0*)	Windows with very high 95th-percentile speed are classified as <i>rail</i> .
stop_thresh	< 0.5	Speeds below 0.5 m/s are considered “stopped” for computing stop ratio.
bus_stop_ratio_min	≥ 0.05	Within the motorized range, higher stop ratios indicate <i>bus</i> .
accel_std_split	< 2.0	Smoother acceleration patterns indicate <i>bus</i> ; higher variability indicates <i>car</i> .

Table H14: Calibrated heuristic rules for transportation mode classification. Thresholds are tuned separately for each dataset using the training split.

*A different threshold was used for Geolife

We evaluated the rule-based model on both the Geolife and MOBIS datasets using the same train–test splits employed for all learning-based models in the main text. The results are reported in Table H15. Despite dataset-specific calibration, the rule-based model achieves only moderate overall accuracy on both datasets (0.3967), with substantial variation in per-class performance.

On the MOBIS dataset, the model exhibits high precision but low recall for the dominant *car* class, indicating that while many predicted car windows are correct, a large fraction of true car instances are misclassified as other modes. Conversely, *walk*, *bike*, and *train* achieve relatively high recall but low precision, reflecting extensive confusion driven by overlapping speed regimes and heterogeneous travel behavior. As a result, the weighted F1-score remains modest (0.4929) despite strong class imbalance.

On the Geolife dataset, the rule-based model performs slightly more evenly across classes but still struggles to distinguish between motorized road modes. In particular, *bus* is almost never correctly identified, while *train* and *walk* benefit from their more distinctive speed profiles. These results highlight a fundamental limitation of heuristic approaches: even when carefully calibrated, fixed rules cannot adequately capture the diversity of urban mobility patterns present in real-world GPS data.

Overall, these findings reinforce our broader argument. While rule-based models are transparent, interpretable, and computationally efficient, they are inherently rigid and brittle. In settings where

large-scale trajectory data are available and mobility behavior is complex, data-driven models that learn representations directly from raw trajectories offer a far more robust and scalable solution.

Dataset	Mode	Precision	Recall	F1-score	Support	Accuracy
Geolife	Bike	0.2818	0.3584	0.3155	3,200	
	Bus	1.0000	0.0000	0.0000	4,863	
	Car	0.0530	0.0871	0.0659	2,251	
	Train	0.4256	0.9512	0.5881	4,119	
	Walk	0.9463	0.4856	0.6418	5,225	
	Macro Avg.	0.5413	0.3765	0.3223		
	Weighted Avg.	0.6400	0.3967	0.3527		
	Overall Accuracy				19,658	0.3967
MOBIS	Bike	0.1087	0.6552	0.1864	17,389	
	Bus	0.1428	0.3550	0.2037	14,474	
	Car	0.9301	0.3278	0.4847	336,860	
	Train	0.0911	0.7243	0.1618	27,607	
	Walk	0.9886	0.4627	0.6303	155,581	
	Macro Avg.	0.4523	0.5050	0.3334		
	Weighted Avg.	0.8581	0.3967	0.4929		
	Overall Accuracy				551,911	0.3967

Table H15: Performance of the calibrated rule-based model on Geolife and MOBIS datasets.

I SpeedTransformer’s Computational Efficiency

Like most deep learning architectures, SpeedTransformer requires substantially higher computational resources than traditional, non-deep learning models. Nevertheless, through our adaptation of the Grouped-Query Attention (GQA) structure, the model achieves comparatively high computational efficiency.

As illustrated in Figure I4, during a full training session with four processes on a single A100 GPU node, the model maintained an average GPU utilization of approximately 67% (peaking at 96%) across all devices. Meanwhile, host memory usage averaged around 52.9 GB (with a peak of 61.9 GB) over a training period of roughly 126.5 minutes. These measurements suggest effective multi-GPU-process utilization and stable memory management, consistent with a compute-bound workload characteristic of Transformer-based architectures.

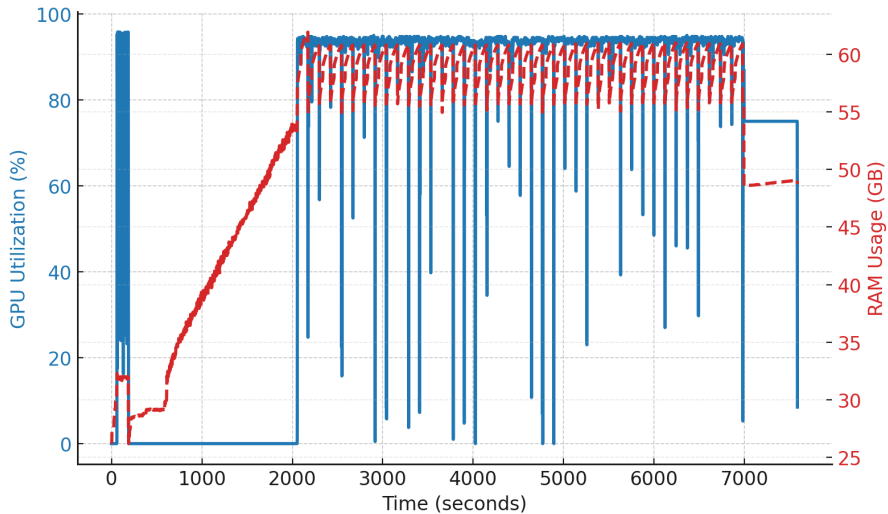


Figure I4: GPU and memory utilization of the Transformer model during training.

J IRB Protocol and Ethics Approval

Following the Committee on Publication Ethics (COPE) guidance, we include our IRB protocol and ethical statement here, concerning our real-world experiment. In respect for conciseness, we summarize our IRB protocol and its approval below.

This study was approved by the Institutional Review Board (IRB) at Duke Kunshan University (DKU) shortly before the carried out experiment. The protocol (version dated June 23, 2022) received clearance to conduct randomized experiments using a WeChat-based mini-program developed by the research team. Participants were recruited from cities in China, through both online advertisements and QR-code posters in focus groups.

Eligible participants (aged 18 and above) provided brief informed consent, consistent with standard practices in the industry, before engaging in the study. The consent process was integrated into the mini-program and clearly stated that no personal identifiers (e.g., name, phone number, WeChat ID) would be collected. Instead, a pseudonymous device ID was used to generate a non-identifiable case ID for analysis. Demographic information is purposefully not collected to protect human subjects' privacy. Minimal geographic and behavioral data were collected for the purpose of estimating participants' daily carbon footprints.

The study involved daily interaction with the mini-program over a one-month period from November 2023 to December 2023, during which participants received varying forms of informational stimulus—ranging from government policy content to scientific facts and social cues. Weekly questionnaires measured participants' willingness to pay for carbon reduction.

Data were stored securely on DKU-managed servers, and all members of the research team were Chinese citizens, in compliance with China's data sovereignty regulations. No audio, video, or photographic data were collected. Participants had the option to donate or receive a small monetary compensation for their time.

This research posed minimal risk to participants and involved no clinical interventions. The IRB ensured that appropriate data security and privacy measures were in place.

We include the full approval letter in the journal's manuscript portal.

K Masking Raw Coordinates as a Privacy Benefit

To demonstrate the potential benefit of our approach, we construct a hypothetical scenario where masking raw original coordinate can preserve individual privacy. Consider a city with a land area of $A = 1000 \text{ km}^2$ and a GPS sampling resolution of $r = 10 \text{ m}$. The number of unique spatial states $N_{spatial}$ is $A/r^2 = 10^7$, yielding a spatial entropy of:

$$H(\text{location}) = \log_2(N_{spatial}) = \log_2(10^7) \approx 26.57 \text{ bits.} \quad (20)$$

In contrast, assuming a speed range of 0–120 km/h quantized at 1 km/h increments (121 states), the speed entropy is:

$$H(\text{speed}) = \log_2(N_{speed}) = \log_2(121) \approx 6.92 \text{ bits.} \quad (21)$$

This indicates that a single speed entry provides less than one-third of the information necessary to resolve a spatial position. This reduction in entropy manifests in much higher k -anonymity [75]: while four spatio-temporal coordinates can uniquely identify 95% of individuals ($k = 1$) [37], speed sequences in dense urban environments can be far less distinctive. Numerous users share near-identical speed profiles due to shared traffic constraints such as synchronized signal timings and speed limits, making individual re-identification from speed sequences orders of magnitude more difficult than from absolute trajectories.

L Temporal Sampling Frequency

We use dense GPS trajectories in this study, primarily obtained through continuous app-based tracking on personal smartphones and mobile devices. This stands in contrast to sparse GPS trajectories derived from geolocated social media posts or sporadic geotagged check-in data. As such, the temporal sampling frequency of our dense GPS data is generally high, though it still varies across datasets. For

all three datasets used in this study, we retained the original sampling rates and did not perform any temporal resampling. Figure L5 shows the distribution of time intervals between consecutive GPS samples in each dataset. By comparing trajectories collected through our *CarbonClever* mini-program field experiment with those from Geolife and MOBIS, we observe variations in temporal granularity. These variations provide a rigorous basis for evaluating model performance.

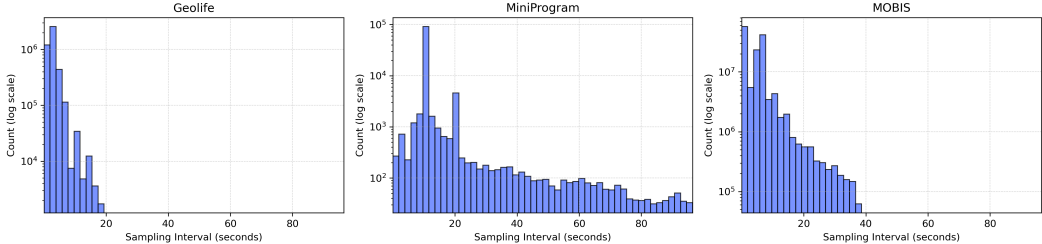


Figure L5: Sampling Frequency Distribution

M Architectural Comparison of Transformer-based Models

The number of trainable parameters in a Transformer-based model is important because it reflects a fundamental trade-off between model performance and computational demand. In general, models with more parameters require greater computational resources and larger training datasets to achieve strong performance. The numbers of trainable parameters for SpeedTransformer and the related Transformer variants are summarized in Table M16. As shown, SpeedTransformer does not contain substantially more parameters than other state-of-the-art Transformer-based mode-detection models.

Table M16: Architectural Comparison of Transformer-based Mobility Models

Model	Pre-proc.	Input	Attention	PosEnc.	Params
SpeedTransformer	Speed Calc.	1D Speed	GQA	RoPE	0.73M
Deep-ViT [59]	Image Gen.	2D Image	Vision MHA	Learnable	0.53M
TMD-BERT [61]	Discretisation	Tokens	Bi-Directional MHA	Learnable	110M

Note: GQA: Grouped-Query Attention; MHA: Multi-Head Attention; RoPE: Rotary Positional Embeddings; Image Gen.: DeepInsight Transform; Params: approximate number of trainable parameters using the best configuration.

N Confusion Matrices and Class Imbalance

We examined the extent to which class imbalance in the training data—specifically the substantially smaller number of observations for *Bike*, *Bus*, and *Train* in both MOBIS and Geolife—contributes to misclassification. Figure N6 reports the confusion matrices for SpeedTransformer on the Geolife and MOBIS test sets, respectively. As is typical across machine-learning algorithms, SpeedTransformer exhibits weaker performance on classes with limited training data, namely *Bike*, *Bus*, and *Train*, relative to classes that are more abundantly represented. Nevertheless, the performance is far from abysmal: per-class accuracy remains well above 50%.

As shown in Fig. N6, the Geolife dataset yields a clear, strongly diagonal confusion matrix, indicating consistent class separation. By contrast, in MOBIS, the *Train* category effectively aggregates several rail- and public-transport subclasses (e.g., train, tram, and metro-style services), whose movement signatures are often highly similar. As a result, predictions for *Train* more frequently diffuse into adjacent public-transport labels.

Moreover, when SpeedTransformer is first trained on MOBIS—the dataset with the largest volume of training samples—and subsequently fine-tuned using a small subset of Geolife and our CarbonClever field-experiment data, its performance remains comparatively strong (Figure N7). Per-class accuracy is generally above 0.9, and even in classes where MOBIS training data may be less well matched to Geolife or the field-experiment test data (e.g., the *Train* class), accuracy still exceeds 0.7.

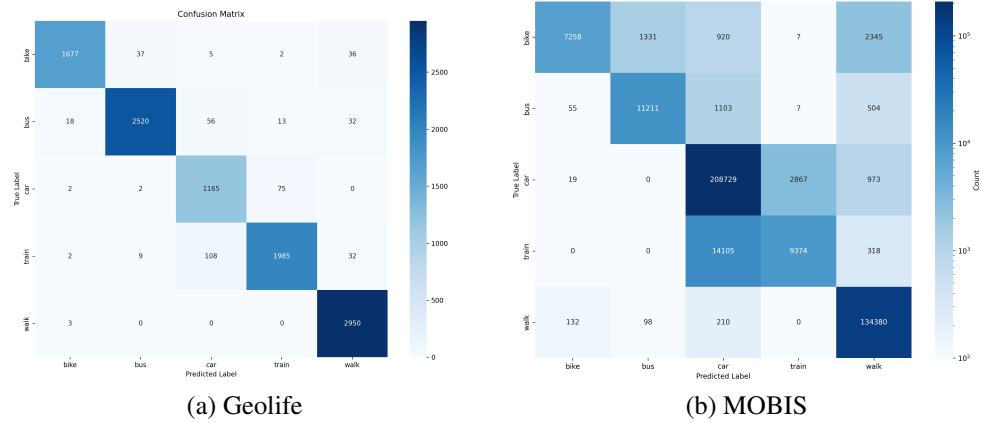


Figure N6: Confusion matrices for SpeedTransformer on the Geolife and MOBIS test sets. Values are raw counts; MOBIS exhibits stronger class imbalance, leading to larger absolute counts.

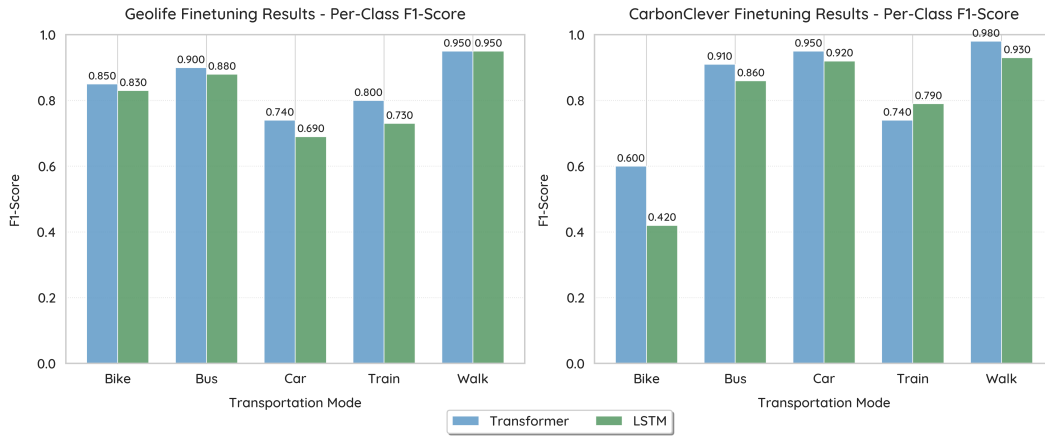


Figure N7: Per class F1-Score for Fine-tuning on Geolife and our real-world field experiment data using SpeedTransformer and LSTM. The SpeedTransformer consistently achieves better results than the LSTM-Attention across all classes in both tasks.

O Failure Analysis: Train Mode Case Studies

Having shown that misclassification is more prevalent for certain classes, we next examine specific failure patterns using the *Train* mode as a case study. Figure O8 contrasts two dominant error profiles for train mode: a *low_speed_confusion* group, which is frequently misclassified as walk or bus and exhibits smooth, gradually increasing speeds; and a *high_speed_confusion* group, often involving car–train mix-ups, characterized by stop–go variability and intermittent speed spikes. Both profiles encompass many distinct trajectories, suggesting systematic patterns rather than isolated anomalies.

Figure O9 further shows substantial overlap in simple summary statistics (e.g., mean and standard deviation) between correctly and incorrectly classified train mode, indicating that such aggregates are insufficient to distinguish the error. As such, the model learns a diffuse representation of the *Train* class, which in turn allows leakage into neighboring public-transport modes. By contrast, Geolife exhibits more homogeneous train trajectories, supporting a sharper and more stable decision boundary for this class.

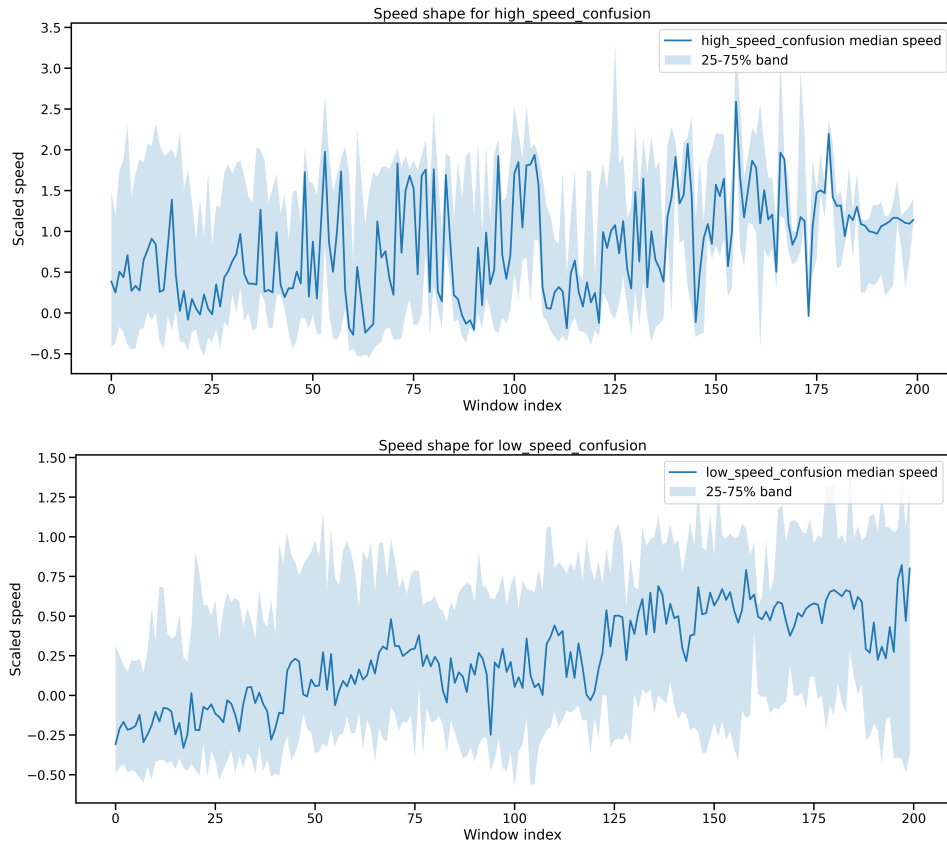


Figure O8: Sequence-level speed dynamics for two dominant train failure profiles. The *low_speed_confusion* profile shows relatively smooth, gradual ramps; the *high_speed_confusion* profile has higher variance with abrupt fluctuations and spikes. Shaded regions indicate the 25–75% interquartile range across sequences.

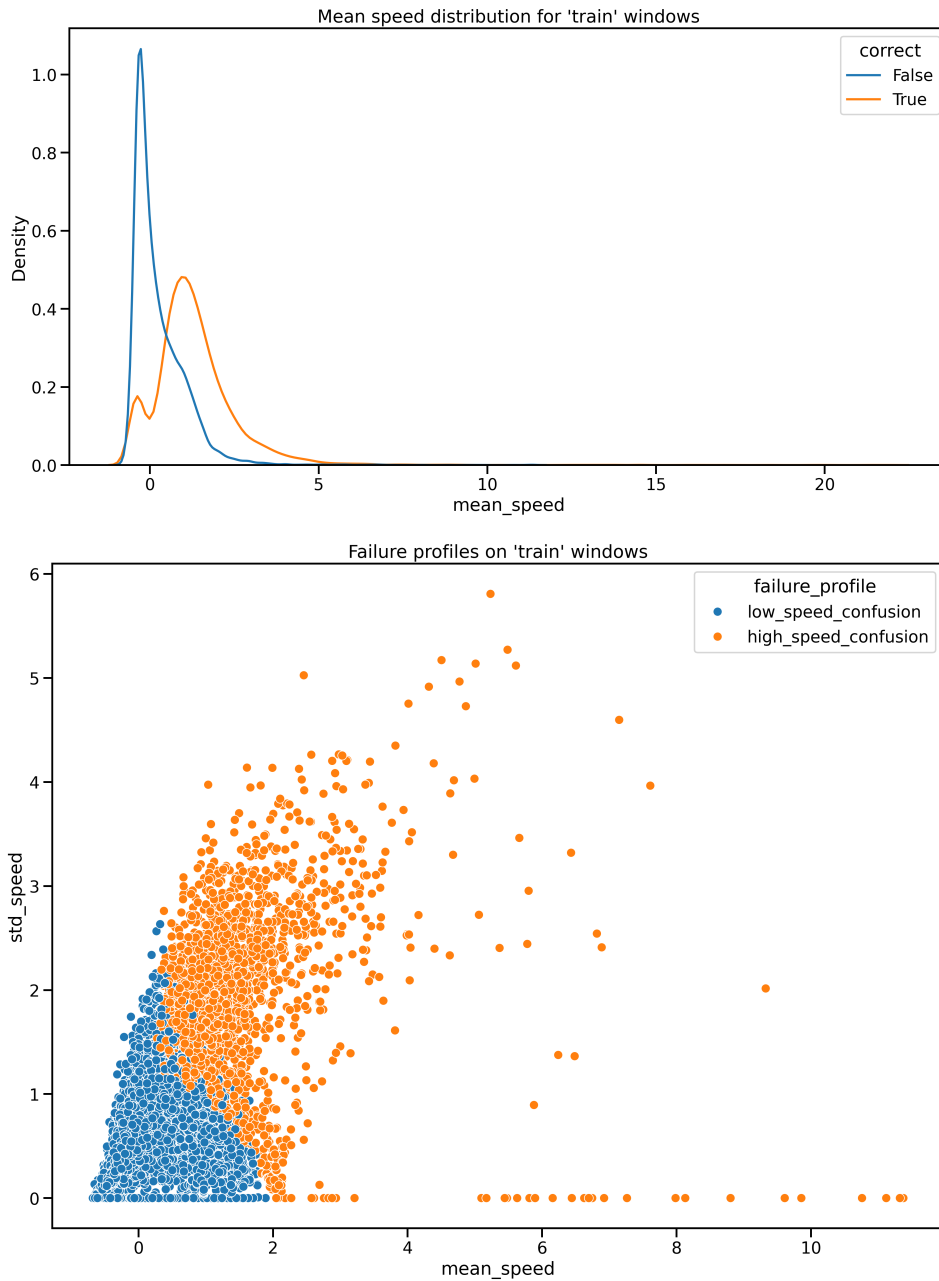


Figure O9: Distributional heterogeneity in train-class speed statistics. Mean speed and joint mean–std representations overlap substantially between correct and incorrect train windows, showing that simple aggregates cannot isolate the failure profiles (*low_speed_confusion* vs *high_speed_confusion*).